Micro-/Nanoscale Robotics for Chemical and Biological Sensing

Liuzheng Zheng[†,a], **Nathan Hart**[†,a], **Yong Zeng**[a]

[a.]Department of Chemistry, University of Florida, Gainesville, Florida, 32611, USA

Abstract

The fields of micro-/nanorobotics have attracted extensive interest from a variety of research communities and witnessed enormous progress in a broad array of applications ranging from basic research, global healthcare and to environmental remediation and protection. In particular, micro-/nanoscale robotics provides an enabling platform for the development of next-generation chemical and biological sensing modalities, owing to their unique advantages as programmable, selfsustainable, and/or autonomous mobile carriers to accommodate and promote physical and chemical processes. In this review, we intent to provide an overview of the state-of-the-art development of this area and share our perspective in the future trend. This review starts with a general introduction of micro-nanorobotics and the commonly used methodsfor their propulsion in solution, along with commonly used methods in micro-/nanorobot fabrication. Next, we comprehensively summarize the current status of the micro/nanorobotic research in relevance to chemical and biological sensing (e.g., motion-based sensing, optical sensing, and electrochemical sensing). Following that, we provide an overview of the primary challenges currently faced in the micro-/nanorobotic research. Finally, we conclude this review by providing our perspective detailing the future application of soft robotics in chemical and biological sensing.

1. Introduction

More than half a century ago, Richard Feynman explored the concept of a swallowable surgeon in his famous lecture entitled *There's Plenty of Room at the Bottom*. In his speech, Feynman imagined the possibility that one day we may have small "mechanical surgeons" able to explore structures in the body as small as the blood vessels and aid in performing both operations and medical diagnoses[1]. Over the past few decades, mechanical and robotic systems have completely reshaped human society. And in present day, state-of-the-art micro- and nanotechnology have greatly fueled the miniaturization of robotic systems, bringing the concept of "swallowing a surgeon" closer to fruition.

Micro-/nanorobots, also referred to as micro-/nanomotors, micro-/nanomachines or micro-/nanoengines by researchers, are functional machines with sizes ranging from nanometers to micrometers. Similar to traditional robotic systems, micro-/nanorobots rely on utilization or conversion of external energy to actuate their autonomous or tethered mechanical movements, which encompass a variety of different actuation mechanisms (see *Propulsion*

[†]These authors contributed equally.

Conflicts of interest
There are no conflicts to declare.

Techniques). Various configurations have also been developed for micro-/nanorobotics, including tubular structure, micro-/nanorod, helical spiral, Janus particle, and biohybrid structures[2]. Through years of multifaceted effort, the field of micro-/nanorobotics has become increasingly more interdisciplinary, attracting researchers from fields ranging from engineering and medicine to even material science and chemistry.

Despite the enormous potential these devices hold and the significant amount of progress accomplished in the past few years, there still exists a few major challenges which stand in the way of future implementation of this technology - the most important of which being locomotion at the micro-/nanoscale.

Any micro-/nanorobot moving in a fluid sample is subject to two major forces: inertial and viscous forces. The Reynold's number ($Re = \rho U L / \mu$ – where ρ represents the density of the fluid, U represents velocity, L represents length, and μ represents dynamic viscosity) provides a ratio of inertial forces to viscous forces present in a flowing fluid. While the movement of larger animals (e.g., fish) in fluids occurs at high Reynolds numbers (where inertial forces dominate), the movement of microorganisms (comparable in size to a microrobot) occurs at very low Reynolds numbers - indicative of an overwhelming viscous forces at hand. With the typical small size of micro-/nanorobots, continuous work must be done to maintain continuous motion in solution[3].

Another challenge presents itself in that micro-/nanorobots are currently not able to be powered using traditional forms of power generation (i.e., batteries, generators, etc.) - meaning that alternative fuel sources must be used, which ideally should be biocompatible and remotely controllable. In a highly viscous medium such as blood (where miniscule amount of inertial force presents), the power supplied must be continuous as well. To overcome these challenges, specific propulsion strategies have been proposed to facilitate their motion in low-Reynolds number environments.

Therefore, in this work, we begin by reviewing the most commonly used propulsion techniques. Taking into account their extremely small size, flexible controllability, and versatile functionalization, micro-/nanorobotics are being increasingly recognized as next-generation platforms for many applications, including biomedicine, biosensing and environmental remediations[4–9]. Specifically, as a platform for "chemistry-on-the-fly", the motion of micro-/nanorobotics in fluids can accelerate reaction processes, which is extremely desirable for the liquid-based sensing. Therefore, in the next section, we focus on the application of micro-/nanorobotics in bio- and chemical sensing. This section is outlined by different sensing strategies – including motion-based sensing, optical sensing, and electrochemical sensing. The following is a survey of state-of-the-art development in sensing-based applications, for which the tasks are based on the sensing of micro-/nanorobotics to specific molecular species, the environment, or to each other.

Even though traditional micro-/nanorobots have indisputable advantages that make them favorable in sensing applications, there are still several long-standing limitations preventing further development in sensing. Meanwhile, as an alternative to conventional rigid robotic systems, soft robotics has rapidly evolved over the past decade to address some of

the critical problems encountered by rigid robotics, including safety, conformability and compatibility[10]. These inherent advantages have led to many instances of soft robotics use in the biomedical field[11, 12]. However, we believe that the participation of soft robotics in bio- and chemical sensing is somewhat underrepresented. Upon comparison with traditional, rigid micro-/nanorobotics, some of the unique characteristics of soft robotics can be potentially used to supplement or remedy the drawbacks of micro-/nanorobotics, especially in the field of bio- and chemical sensing. So finally, we propose the application of (micro) soft robotics in bio- and chemical sensing to push the boundaries of this field even further than before.

2. Propulsion Techniques

Micro-/nanorobots, resulting from their small size, inhabit environments characterized by very low Reynolds numbers and are unable to be powered via traditional power sources. In order for these devices to be able to move in solution, their means of propulsion must be both continuous as well as wireless. In addition, some applications of this technology may require the method of propulsion to be biocompatible as well. In this section, we will describe the most common propulsion methods used in modern micro-/nanorobotics work. Great care will be taken in addressing the mechanism of each method - as well as their advantages and limitations.

2.1 Chemical Propulsion

Using chemical propulsion techniques, a swimming micro-/nanorobot converts chemical energy into kinetic energy for movement. This means for energy conversion is in many cases provided by the use of a metal or metal catalyst - allowing the machine to autonomously propel itself when exposed to fuel in its immediate microenvironment[13]. Since inertia is negligible in an environment characterized by a low Reynold's number, this chemical conversion must be continuous in order for motion in solution to be maintained[14]. There are three main propulsion models of autonomous chemical propulsion: self-diffusiophoresis, self-electrophoresis, and bubble propulsion.

Self-diffusiophoretic motion (Figure 2A)[15] is caused by the presence of concentration gradients (which stem from the asymmetric release of reaction products) around the micro-/nanomotors which work to drive the motors forward[16]. Janus particles have long been associated with this propulsion model - receiving their name from having two hemispheres with distinct chemical/catalytic characteristics[17]. Their inherent asymmetry allows these microspheres to propel in solution via the generation of reaction products on only one side of the particle. In fact, the particle must generate more products than reactants, producing an asymmetric net repulsive interaction with the particle that pushes it forward. A common example of this type of reaction is the catalytic decomposition of hydrogen peroxide - producing both oxygen and water molecules[18]. More than a decade ago, Howse *et al* fabricated polystyrene spheres and coated one side of the spheres with platinum. The metal coating catalyzed the reduction of hydrogen peroxide, allowing the particles to move in a predominantly directed way on a short time scale. This work used the simplest method of producing Janus particles - that being, thin metal film deposition on top of microspheres

typically made of silicon dioxide or polystyrene (however, a variety of other fabrication techniques have been reported)[19].

Self-electrophoretic motion is very similar to the previously mentioned self-diffusiophoretic motion (albeit, more complicated) - stemming from surface reactions which create a heterogeneous distribution of ions in solution. This distribution of ions essentially creates an electric field that works to propel the micro-/nanorobotics[16]. Self-electrophoresis is typically exhibited by bimetallic nanomotors, having one segment dedicated to reduction and the other for oxidation. Calling back to the example of hydrogen peroxide decomposition, an Au/Pt nanomotor can oxidize hydrogen peroxide at the platinum anodic segment and reduce it at the gold cathodic segment - acting in a similar manner to that of an electrochemical cell (Figure 2B)[20]. What happens is the anode produces large amounts of protons and electrons, and an electric field is developed that points toward the cathode. As protons travel towards the cathode, fluid is dragged along with it, which results in movement in the opposite direction with the anode facing forward[17].

Micro-/nanorobots which move via bubble propulsion use the production of bubbles as a means of propulsion and are known for their light weight and small size as well as their high speed and propulsion force in solution (Figure 2C)[21]. Bubble-propelled micro-/nanorobots come in a variety of shapes - including rod- and tubular shaped[22]. The tubular geometry typically involves an inner catalytic surface which decomposes chemical fuel into gas bubbles, which rapidly combine and grow into larger bubbles via effective nucleation and eventually expel out due to pressure. Fabrication of these types of micro-/nanorobotics is typically done using a roll-up technique; however, use of template-assisted electrochemical deposition techniques has been reported as well as a layer-by-layer assembly method (See Section 3. Fabrication Methods). On the other hand, rod-shaped micro-/nanorobotics are completely solid, containing two or more metal segments prepared via an electrochemical deposition technique[17].

In the case of bubble propulsion, a considerable amount of research has been focused on using the catalytic decomposition of hydrogen peroxide by platinum metal to evolve water and oxygen bubbles as a means of high-speed propulsion - with the change in momentum during bubble ejection being speculated to drive motion in the direction opposite of the bubble stream[23]. Interestingly, this change in momentum can be modulated directly via the use of external stimuli (including light, temperature, and acoustic fields) in order to directly control the speed of micro/nanomotors[14]. For example, Li *et al* developed photoactivated TiO$_2$/Au Janus micromotors fabricated by asymmetrically coating gold on the exposed surface of AmTiO$_2$ microspheres - the speed of which could be modulated using the intensity of UV radiation with a response rate less than 0.1 seconds[24]. In an impressive feat, Magdanz *et al* exploited the thermoresponsive nature of poly(N-isopropylacrylamide) (PNIPAM) film, creating flexible, self-propelled microjets which could reversibly fold and unfold into a tubular shape depending on solution temperature. Bubble formation was only observed when the film was folded (cooler temperatures) - as the tubular shape allowed generated oxygen to accumulate into visible bubbles instead of quickly diffusing into the surrounding solution. It was observed that the velocity of the microjets could be controlled via changing the radius of the tube[25]. This concept of speed modulation has been taken one

step further by Wu *et al*, who demonstrated on-demand motion of catalytic microengines dependent upon NIR illumination. Illumination of the microengine with a focused NIR laser could induce a fast thermally modulated motion, reaching a maximum speed of 62 μm/s. However, after leaving the laser spot, the micromotor would soon come to a standstill[26].

Lacking inherent directional motion, the movement of bubble-propelled micro-/nanorobots typically follow random trajectories in three dimensions[14]. However, magnetic material can be incorporated within the structure of the micromotor in order to control the direction of propulsion. For example, Demirbuken *et al* have recently described the fabrication of a self-propelled PAPBA/Pt/Pt-Ni/Pt nanomotor - the direction of which can be changed via use of a magnetic field[27]. The use of fuel concentration gradients has also been demonstrated as a means of directional control[14]. A common criticism of this specific means of propulsion is its prevalent use of biologically incompatible catalysts and fuels (including platinum and hydrogen peroxide), limiting its potential use for *in vivo* and biomedical applications[23]. However, what the method lacks in terms of biocompatibility, it makes up for it, with the low cost associated with the technique as well as easy integration of the technology into the nano scale.

2.2 Magnetic Propulsion

The use of magnetic fields as a means of micro-/nanorobotic propulsion has generated considerable interest in the biomedical micro-/nanorobotics community due to its advantages of remote/wireless operation, deep penetration into the tissues and body, directed propulsion, and low adverse effects on living organisms and tissues (biocompatibility)[13, 14]. The working principle behind this technique can be explained in the following sentences. When a magnetic micro-/nanorobot (typically containing either ferromagnetic materials like Ni, Fe, or Co or paramagnetic materials such as Fe_2O_3) of volume v is placed in an external magnetic field (with B representing the magnetic flux density), the device will become magnetized (magnetization represented using M). If subject to a magnetic field gradient (ΔB), the device will experience a magnetic force (F, either attractive or repulsive). In order to minimize magnetic energy when exposed to the magnetic field, the robot will then experience a torque (T) - causing the robot to orient its body so that it aligns with the magnetic field. The direction of the magnetic dipole moment and the external magnetic field controls the torque. A space-varying (gradient magnetic field) or time-varying (rotating, oscillating or pulsed) magnetic field can therefore be used in order to continuously propel the robot in solution[13, 28].

The equations for the magnetic force (Equation 1) and magnetic torque (Equation 2) of a magnetic object inside of a magnetic field are given below:

$$F = v(M * \nabla) \times B \qquad (1)$$

$$T = (vM) \times B \qquad (2)$$

By carefully adjusting the rotation axis of the magnetic field, the micro-/nanorobot can be steered in different directions. In fact, magnetic fields offer as much as six degrees of

freedom for motion - allowing absolute spatial manipulation depending on the actuation system[28]. Essentially, magnetic forces generated in gradient fields and magnetic torque act in a similar way to fuel sources seen in chemical propulsion techniques in order to cause micro-/nanorobots to continuously move in solutions where viscous forces greatly overpower inertial ones.

There are three main translational mechanisms associated with the movement of micro-/nanorobots undergoing magnetic actuation: corkscrew motion, surface-assisted propulsion, and undulatory (traveling-wave) motion. As discussed in Purcell's famous 1977 paper titled *Life at Low Reynolds Number*, time-symmetric, reciprocal motion (e.g., the swimming motion of a scallop which is dependent on the opening and closing of a single hinge) cannot create a net propulsive force in a highly viscous fluid. Therefore, microscopic organisms must produce non-reciprocal motion in order to produce movement in Newtonian liquids[29]. One of the ways in which non-reciprocal motion can be achieved is through use of a non-symmetric or chiral structure (e.g., a helical structure). In mimicking the corkscrew-like motion prokaryotic cells perform by rotating their flagella, micro-/nanorobotics (either fully helical in structure or consisting of a magnetic head attached to a helical tail) are able to accomplish a similar motion by using external rotating magnetic fields (Figure 3A)[30]. Since a magnetic object, upon experiencing magnetic torque, will align its easy magnetization axis parallel with the direction of a local homogeneous field, a torque that is continuously applied under an external rotating field creates rotational movement of the object's body. This steady rotation can be converted into translational motion - the direction of which is parallel with the axis of rotation of a two-dimensional planar rotating field. The direction of this motion (in terms of forward versus backward) can be changed by simply reversing the direction of rotation of the applied magnetic field[28, 31].

Similar in principle to how corkscrew motion is achieved, surface-assisted motion gets its name from the use of a physical boundary to break spatial symmetry for the purpose of generating a walking or rolling motion of micro-/nanorobots at low Reynolds numbers[31]. These micro-/nanorobots are commonly called "surface walkers" or "surface rollers" and can take on a variety of shapes including nanorods and microtubes as well as Janus particles (Figure 3C)[32]. This type of motion is achieved in viscous solution by magnetically actuating a magnetic micro- or nanostructure lying near a surface using a rotating or oscillating magnetic field - the dynamics and mechanism by which is controlled by a variety of factors including: fluid properties, boundary features, and the degree of confinement. While surfaces have traditionally been flat, movement of micro-/nanorobots on topographic surfaces has been achieved[28]. A notable example is described in Wang *et al* in which magnetic nanoparticles were able to be actuated on top of a sample of uneven biological tissue[33].

The third way in which non-reciprocal motion can be achieved is through non-symmetric actuation. Mimicking the motion of cilia and flagella, an elastic component is typically crucial to achieve traveling-wave propulsion. Magnetic micro-/nanorobots capable of undulatory motion have typically been created by either adding an elastic tail to a rigid head or by connecting nanowires together via flexible segments (Figure 3B)[34]. An oscillating magnetic field can then be used to break temporal symmetry and create an effective net

displacement via the thrust from the backward-traveling wave generated by the flexible structure[28, 31]. For example, Li *et al* created a magnetically propelled fish-like nanoswimmer consisting of a gold segment as both the head and caudal fin, two nickel segments as the body, and three flexible silver hinges linking each segment. When actuated by an oscillating magnetic field, the flexible nickel segments caused the body and fin to periodically bend, generating thrust via traveling-wave motions[35].

However, it is important to note that there are instances where Purcell's theorem does not hold. For example, an object undergoing reciprocal motion in a common Newtonian fluid like water can undergo a net displacement if it experiences anisotropic drag[36]. Non-Newtonian fluids are an entire domain in which the scallop theorem does not hold, and fortunately for researchers, many bodily fluids of interest to application of micro-/nanoswimmers (including blood) are classified as non-Newtonian. With this in mind, work from Qui and team have demonstrated creation of a symmetric magnetic, single hinge "micro-scallop" able to propel in non-Newtonian fluids by reciprocal motion at low Reynolds numbers[37].

2.3 Acoustic Propulsion

With the strong medical interest in developing micro-/nanorobotic systems for applications including drug delivery, minimally invasive surgeries, and biosensing *in vivo*, there has been a great effort to develop biocompatible methods of powering these systems - one of these methods being the use of acoustic energy. The medical field is no stranger to using acoustic waves - with ultrasound machines being a common sight in hospitals throughout the world. Acoustic (or ultrasound) propulsion has emerged as a promising off-board approach to micro-/nanorobot propulsion in the last decade due to its inherent biocompatibility and ability to be used with a wide variety of different particle shapes, sizes, materials and solutions[23, 38].

In this technique, micro-/nanorobots convert excitation energy in the frequency (MHz range) and power (up to several W/cm^2) range into axial movement[39]. However, despite all that has been studied, our understanding of the mechanism of acoustic propulsion is incomplete[13]. Even our understanding of the influence design properties has on the propulsion mechanism is very limited. A few known design requirements include the importance of a motor having shape or density asymmetry as well as the ultrasound intensity and particle size needing to be sufficiently large enough in order to ensure acoustic propulsion dominates random Brownian motion. However, a clear hierarchical relationship between these design parameters has not yet been proposed[38]. For example, the directionality of motors composed of a single material is controlled via the motor's shape asymmetry - whereas for bimetallic motors the directionality is controlled via both the density of its materials as well as resonance mode asymmetries[40].

Multiple mechanisms have been proposed in an attempt to explain propulsion of micro-/nanorods via acoustic waves. An early mechanism proposed that the axial motion of micro-/nanorods could be explained by a process known as "self-acoustophoresis" in which the asymmetric shape of the rods leads to asymmetric scattering of acoustic pressure on the rod's surface to generate directional motion. Around a year later, a newer physical

mechanism was proposed in which metallic rods were modeled as axisymmetric rigid near spheres in a standing acoustic wave and acted as a rigid body which moves in a uniformly oscillating velocity field. Oscillation in the fluid is considered to produce steady streaming on the particle's surface to generate propulsion - the force of this propulsion stemming from the rod's asymmetric shape. This model explained the faster motion of more concave rods as well as the need for a large difference in density between the rods and surrounding medium. Later on, a general mechanism was proposed by Collis *et al* which considers both shape and density effects[39, 41]. Debate around the mechanism for this propulsion technique indicates there is still much more to learn about this technique. A more in-depth understanding of the mechanism behind acoustic propulsion could lead to improved micro-/nanorobot actuation performance as well as a myriad of more efficient micro-/nanorobot designs.

2.4 Light-driven Propulsion

The use of light as a renewable source of power for the movement of micro-/nanobots offers a variety of benefits. A main source of attraction comes from the method's variety of adjustable encoding modes (including wavelength, light intensity and polarization) as well as its high spatio-temporal precision which has proven useful for the actuation of single, multiple, and even swarms of micro-/nanorobots[23, 42]. The possibility of concentrating the beam size down to sub-micron levels offers considerable promise in future applications[13]. However, the limitation of the low penetration depths in tissue could perhaps limit *in vivo* applications of these machines to actuation at near skin positions[23]. Once a locomotive object has been scaled down to a low Reynolds number system, it requires a continuous driving force in order to allow it to move against overwhelming viscous forces. In order to achieve movement, a number of light-driven propulsion schemes have been created, which can be divided into two broad categories: propulsion via electric field and non-electric field driven propulsion.

Propulsion via an electric field typically occurs either via self-electrophoresis or electrolyte diffusiophoresis. In self-electrophoresis (Figure 4B)[43], the electric field needed for propulsion is generated by cathodic and anodic photochemical reactions separated in space which create an asymmetric distribution of ions across the particle. Specifically, this electrolyte gradient stems from the asymmetric generation or depletion of photogenerated electrolyte ions under irradiation. Once generated, the charged particles move in response to the local electric field[42]. A common example can be seen by observing Au-Pt bimetallic nanorods. The oxidation of H_2O_2 preferentially occurs at the anode (Pt) end whereas the reduction of H_2O_2 occurs at the cathode (Au) - leading to a higher concentration of protons near the platinum end and a lower concentration near the gold end. Given a proton's positive charge, an electric field develops, pointing from the platinum end to the gold end - allowing the negatively charged nanorod to move in response to the self-generated electric field.

However, in electrolyte diffusiophoresis (Figure 4C)[44], the cathodic and anodic reactions occur in the same area, generating ions typically on one side of the micro-/nanorobot. Owing to the different diffusivities of cations and anions generated (electrophoretic term), a diffusion-induced electric field can be established along a concentration gradient - creating propulsion. Cations and anions can also interact with the double layer of the charged particle

differently, resulting in a pressure which can move the particle. However, this effect (known as the chemophoretic effect) is usually negligible - with the directions of diffusiophoretic flows largely governed by the electrophoretic effect, unless the diffusivities of the cations and anions are very similar[42]. **Equation 3** summarizes the two effects on particle velocity (U) in the presence of a nearby charged surface wall[16]:

$$U = \frac{\nabla c}{c_0}\left[\left(\frac{D^+ - D^-}{D^+ + D^-}\right)\left(\frac{k_B T}{e}\right)\frac{\varepsilon(\zeta_P - \zeta_W)}{\eta}\right] + \frac{\nabla c}{c_0}\left[\left(\frac{2\varepsilon k_B^2 T^2}{\eta e^2}\right)\{\ln(1 - \gamma_W^2) - \ln(1 - \gamma_P^2)\}\right] \quad (3)$$

where ∇c represents the concentration gradient of a monovalent salt, c_0 represents the bulk concentration of ions, D^+ and D^- represent cation and anion diffusion coefficients, k_B is the Boltzmann constant, e represents the charge of an electron, T is absolute temperature, η is the viscosity of solution, ε represent the solution's dielectric permittivity, ζ_P and ζ_W represent the zeta potentials of both the particle and wall, and γ corresponds to

$$\gamma_n = \tanh\frac{e\zeta_n}{4k_B T} \quad (4)$$

Electroosmotic flow can also occur, depending on the presence of a charged substrate. However, this phenomenon depends on the relative magnitudes of the surface charges on the particle and the substrate. A "competition" between both electrophoretic diffusiophoresis and electroosmosis results in the particle moving in either direction. In fact, in both mechanisms, the generated electric field can induce electroosmotic flow, and the migration speed of the particle in both cases can be estimated using the Helmholtz–Smoluchowski equation for electroosmotic velocity[42]:

$$U = \frac{\varepsilon\zeta E_\infty}{\eta} \quad (5)$$

where U is the migration velocity of the particle, ε represents the solution permittivity, ζ is the zeta potential of the particle's surface, η is the viscosity of the solution, and E_∞ is the electric field.

Non-electric field driven propulsion mechanisms include self-thermophoresis and light-induced bubble propulsion. In self-thermophoresis (Figure 4A), the micro-/nanorobot used is typically coated asymmetrically with light-absorbing materials (typically gold) as a means of encouraging directed motion - as opposed to the enhanced Brownian motion observed when symmetrically coated. The coating process can be accomplished via sputter coating under vacuum (in the case of Janus particles) as well as a template-assisted layer by layer process combined with a seeding-growth procedure (in the case of tube motors, colloquially known as micro-/nanorockets)[42, 45]. Absorption of light by the coating generates a local temperature gradient along the particle, creating a net thermophoretic force proportional to the local temperature gradient (∇T) and the particle diameter (d_p) as described in the equation (6)[46]:

$$F = -C\nabla T(\mathbf{r}, t) \quad (6)$$

where the coefficient $C = \frac{9\pi d_p \eta^2 k_a}{2\rho T k_p}$, d_p is the diameter of a particle, η is the viscosity of the fluid, k_a is the fluid thermal conductivity, k_p is the particle thermal conductivity, and ρ is the fluid density. Simply put, the temperature gradient creates a situation in which the frequency of collisions between one (warmer) side of the micro-/nanorobot and the surrounding molecules is higher than that on the other (cooler) side, thus pushing the motor away in the direction opposite of its heated side[45].

Light-induced bubble propulsion makes use of high-performance photocatalysts (e.g., TiO_2 and WO_3) to generate a directed stream of bubbles via a photochemical reaction. In order to form bubbles, these photocatalysts are typically spatially confined (e.g., tubular structure), allowing gases to accumulate and inhibiting their diffusion in solution. Light acts as a "switch", allowing the reaction to be turned "on" and "off." The release of a jet of bubbles during illumination results in a continuous change in momentum which propels the motor through the solution in the direction opposite from the side of bubble generation[42].

Interestingly, Gibbs and Zhao developed an expression for the velocity of a micro-/nanorobot actuated via bubble propulsion, showing that the velocity is proportional to the concentration of fuel as well as γ^2, which determine how much gas is produced[46]:

$$U \propto N \frac{R_g T \rho v_0}{\mu r P} \gamma^2 \frac{kac}{1 + ax}$$

(7)

where N represents the number of bubbles, R_g is the universal gas constant, T is the temperature, ρ is the density of oxygen gas produced, γ is the liquid's interfacial tension, c is the bulk concentration of H_2O_2 fuel, and α is the Langmuir adsorption constant.

2.5 Propulsion/Control via Multiple Energy Sources

Micro-/nanorobots are not limited to making use of only one of the above-mentioned means of propulsion. In fact, there are quite a few recent notable examples in which motors have been designed with two or more methods of control in mind. These "hybrid" robots incorporate two or more energy sources for navigation and control and are therefore better able to respond to changes in complicated environments, extending their utility in multiple applications both *in vivo* and *ex vivo*[23].

A common example of hybrid micro-/nanorobots includes those which have a main mechanism for propulsion and a separate means of directional control (typically magnetic fields). For example, Wu *et al* have developed micromotors for cancer treatment which rely on the enzymatic reaction of glucose oxidase with glucose as a chemical fuel and the incorporation of magnetic Fe_3O_4 nanoparticles as a means of controlling the robot's direction[47]. Recently, Demirbuken *et al* have described the fabrication of a self-propelled PAPBA/Pt/PteNi/Pt nanomotor - the direction of which can be changed via use of a magnetic field[27]. Using computer simulations, Nitschke *et al* have proposed a biocompatible method for the collective guiding of acoustically propelled micro- and nanoparticles in which a space- and time-dependent ultrasonic field propels the particles, and a time-dependent magnetic field collectively aligns their propulsion directions[38].

However, other micro-/nanorobotics have two or more means of propulsion. A notable example would be the pH responsive mesoporous silica-Pt@Au Janus nanomotors created by Xing *et al*. In hydrogen peroxide solution, these nanomotors undergo self-diffusiophoresis due to the catalytic decomposition of peroxide. However, the solution's weak acidity can cause the disassembly/reassembly of gold nanoparticles - leading to reconstruction of the nanomotor and a change in propulsion mechanism from self-diffusiophoresis to self-electrophoresis. The asymmetric, aggregated gold nanoparticles also permit the generation of a thermal gradient via laser irradiation - leading to an additional self-thermophoresis mechanism as well[48]. Karaca and group have reported gold-nickel nanowires able to undergo both magnetic and acoustic propulsion. In fact, both propulsion methods could be activated at the same time - creating impressive speeds as high as 120 μm/s[49]. Taking inspiration from nature, Shao *et al* have reported what they call "twin-engine" nanomotors based on the structure of stomatocytes in which the enzyme catalase was loaded as well as a hemispherical gold coating. These Janus nanomotors could be exposed to both hydrogen peroxide and near-infrared laser light - creating two competing driving forces and resulting in a "seesaw" motion. Modulation of this "seesaw" effect via changing the peroxide concentration and laser power permitted the ability to switch between motile modes[50]. Similarly, Yuan *et al* have reported creating graphene oxide Janus micromotors having an adaptive propulsion mechanism, allowing the motors to use nearby peroxide as a chemical fuel or magnetic actuation via an external magnetic field[51].

3.   Fabrication Methods

A variety of techniques have been employed over the past few decades to create micro-/nanorobots – with advances in micro-/nanofabrication having made great contributions towards the fabrication of these small-scale robotic devices. Particularly, photolithography as well as certain deposition and etching techniques are extensively used in micro/-nanorobot fabrication – along with other fabrication techniques including additive manufacturing. This section aims to provide a review of some of the most commonly used fabrication methods in micro- and nanorobotics.

3.1   Photolithography

The conventional clean room process of photolithography involves the use of a light-sensitive material (photoresist) and a custom photolithographic mask to create designed patterns on a target substrate. Upon illumination of the photoresist, the material changes its solubility properties, leaving the user with a structure having raised features corresponding to the photomask after development[52]. The resolution of this high throughput technique spans from the nanometer to the micrometer range, offering researchers the ability to create intricate patterns and structures with high precision[53].

Recent work by Wang et al describes the use of a layer-by-layer optical photolithographic technique to produce L-shaped magnetic microrobots (Figure 5A)[54]. Briefly, after cleaning a silicon wafer using a plasma cleaner, a layer of magnetic nanoparticle solution was spin coated and baked on top of the wafer to form the first layer. A photo-crosslinkable chitosan solution was then spin coated on top of the magnetic solution layer and dried

to form a photo-crosslinkable chitosan film. With use of a photomask, the sample underwent ultraviolet light illumination and subsequent development, producing chitosan-based achiral planar microrobots. Similar work reported by Tan and Cappelleri uses both conventional photolithography and two-photon polymerization (TPP) to create helical swimming microrobots[55]. Work by Iacovacci et al demonstrates a method for creating soft microrobots, relying on the use of a two-step, backside exposure photolithographic process - allowing for the inclusion of a radiocompound within the robot's structure to permit imaging[56]. A recent publication by Mu and team reports the preparation of MOF-based microrobots[57]. This method relies on the use of sacrificial photoresist platforms used to help release the robots from the substrate for further treatment after a series of metal film depositions using RF magnetron sputtering. Microrobots of different shapes could be created using photomasks having different designs.

3.2   Template-Guided Electrodeposition

Template-guided electrodeposition typically involves the use of an electric current to reduce metal cations (or conductive polymers) onto the surface of an electrode covered with a porous membrane[53]. This membrane is used to restrict growth to occur solely within the pores. A direct consequence of this growth restriction is that the membrane's pore size can be modulated to create different sizes of micro-/nanorobots. The membrane can then be dissolved after deposition, releasing the robots into solution.

In their bid to create a cargo-delivering micromotor that could be propelled using magnetism as well as a chemical fuel, Li and coauthors used electrodeposition with a membrane template as their fabrication method of choice[58]. Their method first begins with sputtering a gold film on one side of the polycarbonate membrane to serve as a working electrode followed by deposition of an external polyaniline layer. A layer of nickel was continuously deposited in the tube as well as the internal platinum catalytic layer. The gold film could be removed by manual polishing with alumina, and the microrobots were subsequently released after dissolving the membrane in methylene chloride. A similar method was recently used by Lu et al in their publication describing the fabrication of superfast, tubular micromotors powered by ultrasonic waves (Figure 5D)[59]. Ji et al have recently demonstrated synthesis of swinging flexible nanomotors[60]. In their method, the authors use electrodeposition to synthesize the nanomotors in a part-by-part method by sequential electrodeposition of gold, silver, and nickel within an aluminium oxide membrane. The authors remark that their use of template-assisted electrodeposition allowed reproducible mass production of nanomotors.

3.3   Additive Manufacturing

There are currently five main types of additive manufacturing (also known as 3D printing) techniques used to fabricate micro-/nanomotors - those being: direct laser writing (DLW), stereolithography, microscale continuous optical printing, inkjet printing, and PolyJet[61]. However, the most common means of 3D printing microrobots is direct laser writing, which will be the focus of this subsection.

Direct laser writing via two-photon polymerization (TPP) involves the use of a high intensity femtosecond laser source to selectively polymerize photosensitive material in a

preprogrammed three-dimensional path via a nonlinear absorption process[62]. Depending on the resist used, areas of the resin that were either exposed or unexposed to the laser can be removed using developer solution in a way similar to conventional photolithography[63]. While DLW is known to have a relatively slower fabrication speed when compared to other 3D printing technologies, it makes up for it with its superior resolution (100 nm).

Liu et al have recently used two-photon polymerization to permit construction of 3D cavities out of photoresist to serve as negative molds for fabricating complex magnetic microdevices with heterogeneous material compositions and 3D programmable magnetization profiles[64]. The authors claim that by repeating their exposure-molding cycle they are able to integrate multiple materials together and program the individual magnetization direction for the purpose of creating smart microdevices - ranging from magnetic micro-rotors to a micro-cilia array. Interestingly, Alsharhan and team have managed to use DLW to create soft microrobotic grippers within a microfluidic device (Figure 5B)[65]. The grippers could be designed in computer-aided design (CAD) software. Using the exported model, CAM (computer aided manufacturing) software could then be used to produce the path the laser will take during printing. Negative-tone photoresist was then loaded into channels in the microfluidic device, and the grippers could be printed in a serial "floor to ceiling" fashion.

3.4   Glancing Angle Deposition

Conventional physical vapor deposition (PVD) processes involve target materials being vaporized and subsequently deposited onto a stationary substrate of the researcher's choice[31]. Glancing Angle Deposition (GLAD) is a more specialized PVD technique used to produce nano-scale columnar films with controlled shapes and porosities[66]. During GLAD, the substrate is tilted at an angle to the direction of the coating vapor flux and rotated to control the film's characteristics and growth. By varying parameters including the angle of incidence, rate of deposition and rotation of the substrate, it is possible to change the morphology and properties of the desired film with fully three-dimensional control - making the technique very useful for nanostructure fabrication with a variety of materials possible.

Using this approach, Dasgupta et al have developed helical nanorobots which they have proposed for use in fighting bacterial infection in the tooth's dentinal tubules[67]. To fabricate their nanorobots, the authors began by first placing down a seeding layer consisting of pillars made of silica. Then, GLAD was used to grow silica helices onto the seeding layer at a deposition angle of around 5° while the seeding layer was rotated. The diameter of each silica pillar in the seeding layer determined the thickness of the nanorobots, whereas the time and rotation rate of the seeding layer determined their length and pitch, respectively. To form the nanorobot's head, material was deposited in layers using a sequential order - that being: 5 nm of silver, 50 nm of silica, 10 nm of pure iron, and 50 nm of silica without rotation of the seeding layer. Material deposition was followed by controlled rotation of the GLAD platform and deposition of silica until a total vertical deposition thickness of 3 μm was achieved. Similar methods have been reported by Ghosh and Ghosh to create helical nanostructures using polystyrene beads as a seeding layer[68]. Rivas and team have recently reported the use of microrobots to physically manipulate cells[69]. Using GLAD, micro-sized

silica spheres were coated with a 100 nm nickel layer at a 70° glancing angle as a means of making them magnetic for actuation via rotating magnetic fields.

4. Applications in Sensing

In conventional surface-based sensing, roaming target analytes – in free liquid phase or gas phase – are recognized and captured by stationary probes functionalized on a solid surface[70, 71]. In this model, the process is mainly driven by two factors: **1**) the inherent (bio)chemical reaction kinetics between target and probe – including electrochemical transduction, enzyme-based reaction and affinity-based recognition[72] – which is the *chemical* limit of the surface assay; **2**) the transport efficiency of the target analyte onto the reactive surface – determined by liquid topography and fluid dynamics, including diffusion, convection – which is the *physical* limit of the surface assay[73]. In the case of a steady-state liquid, mass transport is fueled by passive Brownian diffusion, or molecular random walk. In the case of flow-through platform (particularly microfluidics) mass transport (as well as heat transfer) can be improved compared to the diffusion-limited process, but laminar flow becomes dominant, leading to the formation of a diffusion boundary layer and limited radial convective flux and mixing[74–76]. The mass transport limitation, being increasingly significant at ultralow concentrations, affects the overall sensing performance, including sensitivity, robustness, and response time. In this regard, enhancing the dynamic flux as a means of breaking the bottleneck of mass transport is always appealing to physicists and chemists. Numerous efforts in vastly diverse approaches have been proposed to improve the reaction efficiency and overcome the relevant issues in fluids, such as external advection[71, 77], active depletion of boundary layer[78], generation of convective flow by electro-thermophoresis[79], herringbone microstructure[80–83], isotachophoresis[84, 85], acoustics induced mixing[86–88] and tuning of probe immobilization[89]. However, in these works, sophisticated engineering of the interface or introduction of advanced molecular mechanism[90, 91] are inevitable, restricting the potential mass production as well as out-of-lab implementations.

As mobile platforms of "chemistry-on-the-fly", micro-/nanorobots offer fundamentally revolutionary solutions for surface-based sensing[3, 92]. On one hand, the motion of micro-/nanorobots – including speed and trajectory – is sensitive to many parameters in the surroundings, thus, the motion can be directly used to reflect the changes in these physical or chemical signals; on the other hand, when functionalized with various probes, the active motions of micro-/nanorobots turn them into "active hunters" that feature enhanced target recognition, enrichment, and detection. Simultaneously, in-liquid mass transport (whether in microfluidics or large liquid reservoirs) can be accelerated due to motion-induced fluid convection and mixing[93], which helps to push the limit in the interfacial recognition events between probes and analytes. In all, micro-/nanorobots can help to break the physical limitations in the previously discussed surface-based sensing platforms, leading to shortened response time and enhanced sensitivity[3, 7]. Other unique properties, including minimized size, large surface area, versatile and enduring functionalization availability, help them to flourish. In this regard, micro-/nanorobots has been adopted in the sensing and detection of a wide variety of analytes, including cells, bacteria, proteins, nucleic acid, biomolecules,

inorganic ions, etc. As an unconventional approach, this section will be introducing these applications based on their different strategies.

4.1 Strategies

4.1.1 Motion-based Sensing

4.1.1 Motion-based Sensing—Having controlled, autonomous motion is one of the most critical parts in the design of micro-/nanorobots. Given that the motion in aqueous environment can be dependent on multiple factors (e.g., concentration of chemical species), any changes in these factors will directly lead to the changes in the motion[3], which makes motion-based sensing the earliest developed and the most extensively studied. In 2009, Wang *et al* proposed a catalytic Au-Pt nanowire for the chemical detection of trace level silver[94] (Figure 6A). In this pioneering work, the existence of Ag^+ will remarkably induce an increase in the average speed of the nanowire, as the silver ions would be absorbed onto the nanowire surface with the presence of hydrogen peroxide. The reduced silver could help to accelerate the electrocatalytic decomposition of the hydrogen peroxide fuel, leading to observably faster motion of the nanowire. Besides Ag^+, other heavy metal ions also have significant effect on the catalytic activities that are responsible for the motion of micro-/nanorobots, which led to following studies that used this mechanism to detect water-polluting metal ions such as lead[95] and mercury[96, 97]. For example, Hg^{2+} could be absorbed onto the Pt surface, which dramatically decrease the moving speed of the nanomotor, and the detection of Hg^{2+} reached very low LOD in the allowable range in drinking water[97]. Furthermore, using pH-responsive gelatin material, the catalytic activity can also be engineered to be responsive to the pH of the circumstance, enabling the motion-based pH sensing application[98].

Following the work of Ag^+ sensing, using the same mechanism, motion-based strategy has been developed for the sensing of DNA[99]. Herein, after the capture of the target strand, a detector probe, which was functionalized with Ag nanoparticle, was added to hybridize with the target strand. Therefore, the amount of Ag nanoparticle was in proportion with the amount of target strand. Transferring into H_2O_2 solution, the speed (or the moving distance of a straight line) of the nanomotor can be readily used to determine the DNA or RNA as low as 2,000 copies per μL. However, the system's application in "real-life" samples was quite limited due to the inactivation of high ionic strength[100]. Similarly, a microtube was fabricated, where the inner Au surface was functionalized with DNA strands[101]. To facilitate detection, the Pt nanoparticle, which was also functionalized with DNA strands, would be conjugated onto the Au surface at the presence of the target DNA. Again, the conjugated Pt could catalyze the decomposition of H_2O_2, resulting in a "signal-on" motion-based DNA sensor. However, the sensitivity of this microtube was low (LOD = 0.5 μM), possibly due to the poor catalytic capability of Pt. To increase the sensitivity, the Ju group employed cyclic alternate hybridization assembly of multiple catalytic units, which improved the motion[102] (Figure 6B). The catalase was attached with 2 partly complementary DNA strands (S1 and S2) that can alternately hybridize with each other. Since each strand was attached with a catalase unit, a multilayer catalase structure can be controllably immobilized on the inner surface of the microtube (i.e., S1/S2…S1/S2), which can efficiently empower the motion of the microtube. In this study, the speed in 2% H_2O_2 solution (~420 $\mu m/s$) was much faster than the last case[101] (210 $\mu m/s$ in 5% H_2O_2), and brought about a detection limit that was 50

times lower. Recently, the same group has also developed a jellyfish-like micromotor[103] – an umbrella-shaped structure with increased sensing surface – that featured easy fabrication and sensitive detection of DNA (Figure 6C).

Some other analytes in motion-based sensing include protein[104], glucose[105] and toxins[106, 107], but these are less representative in motion-based sensing due to the more complicated recognition (e.g., enzyme based reactions) and propulsion process (e.g., Marangoni effect). Interestingly, motion-based sensing was also applied for the evaluation of liquid viscosity or mechanical properties of cells[108, 109]. For example, Ambarish Ghosh *et al* internalized helical magnetic nanomotors into cells, performed precise locomotion of the nanomotor, and found that the motion is strongly sensitive to the local mechanical properties of the intracellular environment[110]. While there are many cases that used magnetic tweezers or magnetic wires for the measurement of intracellular environment[111–113], micro-/nanorobots can provide better maneuverability. Later, this group used a helical magnetic nanomotor as the probe to measure the mechanical properties of cytoplasm and found significant difference between normal cell and HeLa cells[114]. Lin Wang *et al* applied motion-based sensing for liquid viscosity[115], where the measurement of 1.5–7.486 cP viscosity was conducted by a bubble propelled micromotor. An inevitable problem in motion-based sensing strategy is the accurate interpretation of the distance or the speed: it can be imprecise using naked eye or labor-intensive using microscopes, which is improper for commercial use. To address this, several studies have proposed using a smartphone platform as a readout. For example, Shafiee *et al* developed DNA engineered micromotors for motion-based detection of HIV[116] and Zika virus[117] (Figure 6D) using a cellphone. Escarpa *et al* also proposed a Janus micromotor for the motion-based detection of glutathione using a smartphone[118], and proved that the analytical characteristics are very comparable to results obtained using an optical microscope.

4.1.2 Optical Sensing—Optical sensing is a powerful tool and comprises an extremely important category of sensing based on micro-/nanorobots[119]. As aforementioned, micro-/nanorobots can be easily functionalized with various optical probes, and these mobile platforms offer great advantages over static platforms to perform "sensor-on-the-fly"[3, 92]. Here, optical sensing can be discussed in the following categories:

4.1.2.1 Fluorescence: Fluorescence detection is sensitive, cost-effective, and straightforward, making it simple to be coupled with micro-/nanorobotics[119]. Fluorescence detection can be conducted via 2 modes: "on-off" detection, where the analyte quenches the fluorescence previously labelled on the micro-/nanorobot, and "off-on" mode, where the analyte "turns on" the fluorescence signal via some specific molecular mechanism.

"On-off" mode.: The Wang group first incorporated quantum dots (CdTe) onto the outer surface of a tubular micromotor, which employed binding-induced quenching to monitor Hg^{2+} in real time[120]. The response time is very short (12s for 3 mg/L Hg^{2+}); however, the sensitivity is not very high (LOD 0.1 mg/L). In another study, a Janus micromotor was coated with dye that allowed instantaneous determination of sarin and soman simulants[121]. Here, the fluorescence of the moving micromotors was completely quenched by sarin and soman simulants while the fluorescence of the static micromotors barely changed, which

demonstrated the increased rate of collision between the moving micromotor and analytes. The Pumera group fabricated a photoactivated tubular micromotor using C_3N_4, which was used for optical monitoring of heavy metal and concomitant removal[122] (Figure 7A). This material possesses inherent fluorescence, eliminating the need to label with fluorescence dyes. After the adsorption of heavy metal ions, the auto fluorescence could be greatly quenched due to the transfer of a photogenerated electron, enabling the rapid sensing of Cu^{2+}. Yang *et al* fabricated a tubular micromotor where the Eu-based MOF material was used for the sensing layer[123] (Figure 7B). The fluorescence emission of the micromotor can be completely quenched by Fe^{3+}, leading to a detection limit of as low as 0.15 μM, which is lower than LODs achieved in other similar works. Similar techniques have been applied in many other research areas, including the sensing of mycotoxin in food samples[124], enterobacterial contamination[125], nitro explosives[126] and gas molecules[127].

"Off-on" mode.: On the other hand, the "off-on" detection methodology offers more intuitive analytical results - even though the transduction process is more complicated as it usually involves the spatial separation of fluorescent dye and quenchers. The Wang group devised a gold nanowire carrying dye-labelled single-stranded DNA and graphene oxide (GO)[128] (Figure 7C). Using ultrasound propulsion, the nanomotor can be internalized into cells easily and safely. The fluorescence of the dye, which was initially quenched by GO due to the $\pi - \pi$ stacking interaction, can be "turned on" when the single strand DNA was hybridized with target miRNA-21 and separated from GO, leading to sensitive miRNA detection in a single cell. Compared to static condition, the hybridization efficiency was observed to be improved due to the nanomotor movement and was directly related to the applied ultrasound and nanomotor speed. A very similar work by this group used a reduced GO/Pt tubular micromotor to carry dye-labeled ricin B aptamer, which enabled real time "off-on" fluorescent detection of ricin B[129]. MoS_2 also has a delocalized electron network that can facilitate the $\pi - \pi$ stacking interaction and has therefore been used to fabricate tubular micromotor with multiple capabilities, including "off-on" fluorescent detection of miRNA-21 and thrombin[130]. WS_2 can also quench the fluorescence (e.g., from rhodamine) via electrostatic and hydrophobic interactions, which was applied in a Janus micromotor for the "off-on" detection of bacterial lipopolysaccharides[131]. Additionally, the WS_2 micromotor had a rougher surface morphology than the MoS_2 micromotor, which allowed increased probe loading and better sensing performances[132]. However, in these works, the fluorescence signal was "turned on" by separating the dye from the quencher, which means the fluorescence signal was not concentrated on the micro-/nanorobot but rather dispersed in the aqueous solution. This will impose possible difficulties in the observation of the fluorescence signal and in real applications. To focus the fluorescence signal on micro-/nanorobots, other mechanisms have been introduced. The Li group grafted mannose on a Janus micromotor, which can instantaneously capture E. coli due to the recognition of FimH proteins[133]. Meanwhile, the specific binding will initiate aggregation-induced-emission (AIE) effect of tetraphenylethene (TPE) derivatives, so the fluorescent Janus micromotor can be "turned on". The same group also applied TPE-T (thymine conjugated on tetraphenylethene) and FITC-G (guanine conjugated on fluorescein isothiocyanate) on a Janus micromotor[134] (Figure 7D). The binding between the fluorophores and aptamer induces aggregation-caused-quenching (ACQ) effect on FITC and

aggregation-induced-emission effect on TPE, where only blue fluorescence was observed. When circulating tumor cells are captured by the micromotor, the blue fluorescence of TPE would be reduced while the green fluorescence of FITC would be restored. Therefore, the ratio between the blue fluorescence and green fluorescence can reflect the amount of CTC, resulting in an interesting "ratiometric" fluorescence detection. Fei Peng and group have functionalized a magnetically driven helical hydrogel micromotor using a monomeric cyanine dye, SYBR Green I, which emits fluorescence upon combining with double-stranded DNA, allowing the fluorescence signal to be observed on the body of the micromotor[135]. Some signal amplification strategy could be introduced, for example, an entropy-driven signal amplification method was used for the detection of miRNA, where the paired target strand would be replaced by a fuel DNA, so the target strand can enter the next round of displacement reaction, achieving the effect of cascade amplification[136]. Reasonably, a smartphone was also introduced for the accurate and convenient readout of the fluorescence detection[137].

4.1.2.2   Colorimetric Sensing: Colorimetric sensing is widely applied in many detection methods, including immunoassays[70]. The Wang group presented the first antibody-functionalized micromotor for capturing and transporting protein between reservoirs in microfluidics[138]. Here, the multistep immunoassay was conducted by magnetically directing the micromotor to separate reservoirs for different events (i.e., capturing of antigen or binding of secondary antibody), simplifying the total process of immunoassay. However, colorimetric analysis wasn't applied in this case. Shortly after, Merkoçi group applied micromotors in a microarray immunoassay and proved that the mass transport was improved by the mixing effect from the micromotor, which resulted in a relative increase in signal intensity of up to 3.5-fold[139]. However, the antibody was functionalized on the microarray slides, and the micromotor only functioned as an additional mixer. Ju's group used an antibody-functionalized micromotor to capture cancer biomarkers (AFP and CEA)[140]. The authors used glycidyl methacrylate (GMA) microspheres modified secondary antibody to specifically recognize the captured biomarker, so the target concentration can be visualized by tag counting or motion speed of the micromotor in only 5 minutes. In another work that used the microscale tags[141], a multiplexed immunoassay of different model proteins was achieved by a micromotor functionalized with different capturing antibodies. In 2017, the Wang group performed ELISA of cortisol on micromotors[142] (Figure 8A). It was demonstrated that the signal intensity from the moving micromotor in 30s was 3-fold higher than that from a static micromotor in 1 minute. Using antibody-attached HRP to catalyze TMB/H_2O_2, rapid, naked-eye detection was accomplished, and here, H_2O_2 was used as both the fuel of the micromotor and the visualizing reagent of the detection. Yong Wang *et al* presented magnetic nanobots as maneuverable immunoassay probes[143]. Instead of self-propulsion, this work utilized magnetic field-induced spinning of the magnetic rod to improve the mixing efficiency, and the resulting fluid flow had been well simulated. Furthermore, they developed a Helmholtz coil for automated and high-throughput analysis of samples in 4 96-well plates. Together with an impressive limit of detection (0.18 ng/mL) and short assay time (< 1 h), this work demonstrated the great potential in applying micro-/nanorobots towards immunoassays. Other types of immunoassays, including fluorescence immunoassay[144], electrochemical immunoassay[145] motion-based immunoassay[117] were also

applied on micro-/nanorobots. Despite immunoassays, colorimetric sensing was also applied to the sensing of glucose[146] or phenylenediamines[147], based on micro- or nanomotors.

4.1.2.3 Surface-enhanced Raman Spectroscopy: Surface enhanced Raman spectroscopy (SERS) is one of the most sensitive techniques in chemical and biological sensing[148], where the signal intensity is amplified by the enhanced electromagnetic field generated from localized surface plasmons. Di Han *et al* developed a catalytic tubular micromotor to capture Rhodamine 6G along with SERS sensing[149]. The outer layer of the micromotor is gold, which can absorb R6G by electrostatic force and can be used as an excellent SERS substrate. Here, the signal from the moving micromotor was 5 times higher than that from a traditional static setup due to more molecules being collected by the moving micromotor. Yong Wang *et al* fabricated a matchlike nanomotor with a AgCl tail[150]. Upon UV irradiation, AgCl would be decomposed and produce H^+ and Cl^-. This would generate an electric field pointing towards the head of the structure, leading to light-triggered self-diffusiophoresis of the nanomotor. The body of the nanomotor was silica-coated Ag, and due to the encapsulation of the inert silica shell, shell-isolated enhanced Raman spectroscopy (SHIERS) sensing of crystal violet and MCF-7 cells was achieved. The signal compared with that from the static condition was 6.2 times higher. The Pumera group fabricated a nanomotor with simple Ag/Au core shell[151], enabling real-time, sensitive detection of picric acid with detection limit of 10^{-7} M. Hotspot engineering – an efficient method to fabricate high-performance SERS substrates – was also applied on a magnetic micromotor[152] (Figure 8B). Benefitting from both hotspot engineering and the rotation-caused active molecular enrichment, ultrasensitive sensing of R6G (detection limit 5×10^{-10} M) was demonstrated. Xiaojia Liu *et al* grafted a thermoresponsive polymer (PNIPAM) on the outer surface of hollow mesoporous silica nanoparticles[153], forming a controllable "gate" for the in situ sampling. Gold nanodots were encapsulated within the nanoparticle as SERS sensing probe. When the "gate" was opened, analytes would be introduced into the hollow nanoparticles for subsequent SERS sensing.

4.1.3 Electrochemical Sensing—Electrochemical sensing is a sensitive method that is widely used, especially for analytes that can undergo redox reactions[154]. Reasonably, it has also seen application in sensing based on micro-/nanorobotics. In some studies, micro-/nanorobots were only used as a controllable mixer of the existing liquid-based sensing scheme. For example, the Wang group used Janus micromotors on printable sensor strips to induce mixing and improve the mass transport in the amperometric detection of nerve agent[155], where the sensitivity was increased 15 times. Rojas *et al* used Janus micromotor in the electrochemical analysis of diphenyl phthalate (DPP) in complicated matrices[156], increasing the sensitivity over around 20-fold. Lei Kong *et al* utilized Janus micromotors in the electrochemical detection of glucose and improved the sensitivity with respect to the concentration of micromotors introduced[157].

In other studies, micro-/nanorobots were used as mobile platforms to capture analytes for subsequent electric readout. The Pumera group published work that developed the remote monitoring of micromotors using a voltametric method[158, 159] and a chronoamperometric method[160], which could be possibly used for electric readout of motion-based sensing.

Escarpa *et al* functionalized a magnetic micromotor with antibodies to immunologically capture C-reactive protein in very low sample volumes and then collect the micromotors onto electrodes for sensitive amperometric readout[145] (Figure 8C). Chun Mao *et al* proposed a Mg-based magnetic Janus micromotor for miRNA and protein detection[161]. Here, the micromotor was actuated by the reaction of Mg and water to generate H_2 and Mg^{2+}. The micromotor was functionalized by the trapping agent with Mg^{2+}-induced nuclei acid fragment, when Mg^{2+} ions were generated, this fragment would be cut to release the target and fragments in cycles to realize signal amplification. Finally, a funnel-type electrochemical detection device was used to ensure full recovery of the recognizing agents.

4.2   Sensing-based Applications

Even though this section is primarily focused on the sensing application of micro-/ nanorobotics, other interesting applications – based on and beyond sensing – are also necessary to be included and discussed here to provide a comprehensive overview and prospect. Being mobile platforms for "chemistry-on-the-fly", the advantages in minimized sizes, large surface area, and tunable functionalization availability make micro-/nanorobotics superior in these cutting-edge applications.

4.2.1   Target Isolation, Transport, and Delivery—Resulting from controlled motion, micro-/nanorobots can be further used for isolation, transport, or delivery after recognition of target analytes, which is the most extensively studied application[162]. The Wang group have developed a series of micromotors functionalized with specific receptors for the isolation of bacteria[163], protein[164], nucleic acids[165], and cancer cells[166]. Other than receptors, molecularly imprinted polymers (MIPs) were also used for target recognition and transport[167, 168]. They also fabricated a helical nanomotor coated with a layer of natural platelet membrane, which had anti-fouling capability in biological environment and was used to capture and transport platelet-specific toxins and pathogens[169]. Another similar work was the coating of a hybrid membrane on an acoustically-actuated nanomotor for recognition and detoxification of different biocontaminants[170].

More important is the ability of micro-/nanorobots to controllably deliver target (e.g., genes, drugs, imaging agents) into tissues or cells. Nelson *et al* functionalized magnetic helical micromotor with lipoplexes, which could be loaded with plasmid DNA. The micromotor was steered wirelessly to come into contact with cells and could easily fuse or incorporate into cells, allowing the transport of DNA as gene therapy agents[171]. Peer Fischer *et al* fabricated a nontoxic and biocompatible nanomotor with a helical silica body and ferromagnetic FePt tail and functionalized it with polyethyleneimine[172]. This allowed the nanomotor to carry plasmid DNA and transfect target cells. Renfeng Dong *et al* used an ultrasonically-propelled gold nanomotor to deliver model antigen (ovalbumin) into cells to trigger an immune response[173]. Previously, the acquired response was limited since the internalized exogenous antigens are mostly degraded by lysosome. However, in this case, the controlled nanomotor could be controlled to escape capture via lysosome, which improved the expression level of antibody. The Wang group also used RBC-PFC (red blood cell membrane-coated perfluorocarbon nanoemulsion) to coat acoustically-driven gold nanomotors for active intracellular oxygen delivery, which found application in maintaining

the viability of cells[174] (Figure 9A). The oxygen release rate could also be tuned by ultrasound intensity, and this model could be used for the delivery of other therapeutic gas molecules.

Due to the ability to penetrate deep tissues and complex structures, researchers have also functionalized micro-/nanorobots with imaging agents for applications in medical imaging[162, 175]. For example, Xiaoyuan Chen *et al* fabricated a helical magnetic microswimmer coated with polydopamine (PDA)[176]. The PDA coating enhanced the photoacoustic signal and photothermal effect, and meanwhile, it also had an innate fluorescence quenching property that led to diagnosis with fluorescence probes. Combined, the microswimmer had real-time photoacoustic image tracking and theragnostic capabilities for the treatment of pathogenic bacterial infection. Li Zhang *et al* proposed a biohybrid magnetic microrobot based on microalgae[177], which had desirable functional attributes from two elements: on one hand, the inherent property of microalgae led to in vivo fluorescence imaging and remote sensing; on the other hand, the coated magnetite (Fe_3O_4) allowed for precise motion control as well as deep in vivo magnetic resonance imaging where fluorescence imaging is not possible. This biohybrid magnetic microrobot could therefore be used in imaging-guided therapies. Further, intelligent self-guided micro-/nanorobots that can respond to different taxis are being developed[178], and they are specifically appealing in applications involving tumor tissues that can establish chemical taxis in their surroundings. The targeting process includes carrier penetration through various biological barriers, such as blood-brain barrier, gastric mucosal barrier and cell membrane barrier[2]. Using a biohybrid microrobot, Schuerle *et al* developed a magnetic bacteria-based micromotor[179]. Using Magnetospirillum magneticum strain as a model organism, the microrobot can undergo magnetic torque-driven motion followed by spontaneous taxis-based navigation, which can improve the infiltration through tissue barrier to deliver liposomes. Here, the rotating magnetic field showed several advantages over a conventional directional magnetic field - including moderate strength at clinical scales, better motion control, improved translocation, increased extravasation of liposome conjugate and enhanced intratumoral transport. The Gao group developed a photoacoustic computed tomography (PACT) microrobotic system, where micromotors were first enveloped in a microcapsule[180]. Due to the protection of the microcapsule, it can withstand the erosion of the stomach fluid, and the motion in vivo can be visualized using PACT. The release of the drug-loaded micromotors can be triggered by near-infrared irradiation, making this system dually capable of imaging and controlled delivery of drugs.

To conclude, micro-/nanorobotics offer multiple advantages compared to conventional methods and platforms in targeted isolation, transport, and delivery, and some of these aspects are still not fully discovered. In the next few years, more significant applications can be expected to fundamentally promote the development of precision medicines[108].

4.2.2 Pollutant Removal—Micro-/nanorobotics has been investigated as mobile reactors for many applications, and this is specifically attractive for environmental applications where pollutants or other hazardous species can be removed immediately after recognition by micro-nanorobotics[6, 181–183]. The Pumera group developed a single-component $BiVO_4$ star-shaped micromotor. Using this material, photocatalytic generation of

reactive oxygen species (ROS, including superoxide and hydroxyl radicals) killed yeast that had been captured on the surface of the micromotor[184]. The same group also fabricated a MOF-based self-propelled micromotor for efficient preconcentration and removal of radioactive uranium (96%)[185], because MOF-based materials have excellent adsorption capacity of uranium. MOF was also applied in another biocatalytic nanomotor with boosted removal efficiency for both inorganic metal ions and organic per- and poly-fluoroalkyl substances (PFAS)[186], as a result of the adsorption capability of the MOF substrate and the mass transport increased by micromotor motion. Xing Ma *et al* used a bilayer tubular micromotor for simultaneous contaminant monitor and remediation[187] (Figure 9B). The inner layer was TiO_2 doped with Pt and Fe_3O_4 for improved motion control, while the outer layer was mesoporous silica ($mSiO_2$) for pollutant adsorption. The internal TiO_2 shell exhibited photocatalytic activity that can help to accelerate the degradation of the collected pollutants. Recently, a low-cost tubular micromotor based on kapok fiber (KF, which is rich in nature) matrix was developed by them for water treatment[188]. MnO_2 deposited on the micromotor was used as a catalyst for bubble-generation propulsion, and together with the coated Fe_3O_4 nanoparticles, the induced Fenton reaction can greatly enhance the removal efficiency of methylene blue.

4.2.3 Swarm Behavior—Swarm behavior is very common and vital in nature, and it has long inspired researchers in micro-/nanorobotics[189]. As tiny carriers of "chemistry-on-the-fly", the coordinated and intelligent swarm behaviors of these individuals can overcome some limitations of single micro-/nanorobots (including limited volume and power) and thus can be revolutionary to a variety of applications ranging from drug delivery and imaging to microassemblies[190, 191]. Furthermore, they may show signal enhancement or propulsion enhancement[119]. In nature, the swarm behaviors rely on communications among individuals, and similarly, at the micro/nanoscale, the agents rely on the chemical or physical interactions and perceptions so that individuals can act accordingly with group members. The most popular example is the magnetic active swarm[192], as a magnetic field is easy to apply and dynamically control, and in this way, the magnetic interactions among individuals and the resulting swarm configurations can be dynamically engineered, such as ribbon, chain, and vortex[193, 194]. Zhang group utilized an oscillating magnetic field to induce the specific swarm patterns of paramagnetic nanoparticles under equilibrium[195]. Depending on the applied magnetic field, the nanoparticles will be attracted to form clusters, and adjacent clusters will attract each other to form ribbon-like bundles. By tuning the oscillating frequency and amplitude ratio, different swarm patterns were presented. Interestingly, the fluidic repulsive interaction also needed to be taken account of in the formation of the swarm pattern (this can be regarded as medium-induced swarm, which was investigated in another work that investigated the generation and actuation of microrobot swarms in bio-fluids[196]). The microswarm facilitated controllable generation, reconfiguration, and navigated locomotion. In another work, they utilized the dipole-dipole interaction between paramagnetic nanoparticles to organize chain-like microswarm with reversible elongation. The nanoparticles were coated with gold shell to be conductive, and this magnetic microswarm can be used to repair broken electrical circuit, which is very similar to ant bridge[197]. More applications based on magnetic microswarms include targeted elimination and disruption of biofilm occlusion[198], selective in vivo embolization that can mitigate some

complications in previous studies (such as blindness or stroke)[199], dental treatment[200], and targeted delivery in blood vessels[201].

While in most cases, the physical interactions (i.e., magnetic interactions and medium-induced interactions) dominate swarm behaviors, the role of surface chemical properties was also investigated. Bradley Nelson *et al* examined the effect of surface wettability in the controllability of magnetic helical micromotors swarming[202] (Figure 9C). The helical micromotors can be typically actuated by rotating magnetic field, and there existed a step-out frequency ($\omega_{step-out}$) when the magnetic torque on the micromotor no longer followed the increasing frequency of the rotating magnetic field; after that, the drag torque on the micromotor still increased and became higher than the magnetic torque, so the moving velocity started to decrease. As the surface with higher hydrophobicity will experience significantly lower drag force, it was reasonably found that the more hydrophobic micromotors will have higher step-out frequency. In this work, they used this phenomenon to selectively control a group of helical micromotors (with certain wettability) within a larger swarm by applying rotating magnetic fields with different frequencies. In light of the COVID-19 outbreak, Pumera's group utilized the collective behavior of antibody-functionalized magnetic microrobots for the immunoassay of SARS-CoV-2 virus[203]. After the "on-the-fly" recognition of spike protein, multiple microrobots show collective self-assembly and form 3D-staggered chains, which can improve the detection performance as it can travel through larger area with greater forces. Finally, the aggregates were characterized by hydrogen evolution reaction (HER) of the silver-shell/gold/core nanorods attached to the secondary antibody. Recently, they also used a magnetotactic bacteria, Magnetospirillum magneticum strain AMB-1 (M. magneticum AMB-1), as the building blocks for a microrobot swarm[204]. By applying a magnetic field, the bacteria would be synchronized and move in a swarm manner, which is due to the biosorption property with each other (but the mechanism wasn't thoroughly revealed). Nevertheless, compared to the popularity of the study in micro-/nanorobot swarm, the cases that focus on the influence of chemical and biological properties are still very rare, and the importance may be underestimated. Furthermore, other than magnetic control of the microswarms, acoustic control, optical control and electrical control were also summarized[191], and the advances in the swarm behaviors represent the frontier of the research field and can push the boundaries for next-generation applications.

5. Challenges and Perspectives

As "sensor-on-the-fly", micro-/nanorobots have several distinct advantages for liquid-based applications: minimized volume and size, large surface area, controlled movement, versatile functionalities, and most importantly, the accelerated physical and chemical processes caused by the actively enhanced mass transport. All these factors contributed to the breakthrough of surface-based sensing over the past few years. Other applications based on sensing, such as target transport and delivery, environmental remediation, and swarm behaviors, are also being rapidly developed and have proven the considerable promise of micro-/nanorobotics in broad research and industrial areas.

However, the summarized examples are still confined in laboratory settings, and limitations from nearly every aspect are restraining its widespread availability like ELISA or LFA strips. **First**, the cost of materials and fabrication is high. As unconventional robotic systems, the fabrication of micro-/nanorobots heavily relies on cleanroom-based fabrication techniques, which is the primary source of the overall cost. The starting materials are usually precious noble metals or synthetic polymers, which are not commercially affordable. Therefore, the innovation to apply cheaper materials and simpler fabrication methods can significantly promote the scalable production and the commercial application of micro-/nanorobots. At the same time, the operating instruments and procedures of micro- and nanoscale robots are also costly. **Second**, the compatibility and biosafety, including the potential hazard of their propulsion reactions and biodegradability of the robot body itself, has only been partially addressed in some studies attempting to use degradable materials[188, 205–208]. For example, chemically propelled micromotors are easy to devise, but most of them use toxic H_2O_2 as fuel and involve unwanted byproducts, which are clearly detrimental to biological molecules or reductive substances. At the same time, the long-term immune response of these exogenous robotics for in vivo application needs to be further investigated[2, 209], not to mention that some propulsion methods (such as bubble-propelling) are impossible to be applied in vivo. With these problems at hand, it's hard to foresee the real change from micro-/nanorobotics, but in general, this field is moving toward more bio- and eco-friendly propulsion strategies, especially with the development of biohybrid robotics[210]. **Third**, the controllability of micro-/nanorobotics regarding the simplicity of operation is limited. In most of the reported cases, these two figures of merit must be compromised for the other. For those with autonomous navigation and propulsion, controlling the free robotics for multistep assay (such as signal readout) is a liability; for those propelled by external field, the operating procedures are demanding and complex, posing serious challenges for out-of-lab availability. Most of the advantageous controlling methods of the motion were accomplished in vitro or on-chip, but for in vivo applications, the effective control on the motion can be threatened by the non-Newtonian movement, high ion strength and heterogenous biofluid compositions and relatively low chemical concentrations[8]. The collective swarm of individual robotics had exhibited distinct controllability, but the underlying mechanisms are still not fully revealed[211]. Considering these challenges, enormous effort is expected in the optimization among fabrication, functionalization, and controllability of propulsion (also navigation) strategies for future applications.

Soft Robotics-based Sensing

Meanwhile, the last decade has also been witness to unprecedented and substantial developments in soft robotics[10, 212–214], which is an expanding subfield of robotics that applies soft matters as the building materials. The shift from rigid materials to soft materials can make dramatic changes to the robotic system in terms of: continuity in configuration, deformable and flexible interfaces, durable and elastic geometries, increased degrees of freedom in motions, and more importantly, the growing attention to biomimicry, as well as the effective mutual interactions between the compliant robotic systems and life systems[212]. Therefore, soft robotics have unparalleled adaptability to perform more delicate tasks that were not approachable by the rigid counterparts[215]. Soft robotics is being introduced into

multiple research fields and has already revolutionized several biomedical fields, including wearable assistive devices, prostheses, and surgery tools, etc[12]. However, the application of soft robotics in sensing, especially bio- and chemical sensing, is still underexplored[216, 217].

Specifically, soft robotics have some unique features that make them extraordinary for biomedical research and applications. **First**, the fabrication and materials of soft robotics are generally low-cost. Most soft robots are composed of elastomeric polymers such as PDMS and Ecoflex, which are both cost-effective as well as readily available for purchase. Even when integrated with advanced functional modules such as flexible circuits or stimuli-responsive polymers, the overall cost is still low. The fabrication of soft robotics typically involves a variety of low-cost and commercially available methods, such as 3-D printing[218], template molding[219], or combined[220]. Recently, P-T Brun et al proposed a bubble-casting method for the fabrication of soft actuators with various geometries, sizes and aspect ratios, which is very flexible, convenient and rapid[221]. **Second**, as an alternative to hard robots, soft robots are typically more deformable, lightweight, and safer for biomedical applications. For example, as medical devices, safe interaction with the human body is emphasized, and as assistive wearables, compliant contact and similar mechanical properties with human tissue are prioritized[11, 12]. Even in non-biomedical applications, this property is still quite desirable to perform more delicate and subtle tasks[222]. Furthermore, the superior conformability endows soft robots with more degrees of freedom and controllability to navigate across obstacles and unpredictable changes in unstructured environments[223], so the locomotion in highly confined and delicate spaces (e.g. microfluidics and in vivo cases) is within reach[224]. **Third**, soft robotics have improved adaptability and agility in the actuation and movement compared to micro-/nanorobotics[225]. Micro-/nanorobotics are more frequently referred to as micro-/nanomotors by some researchers because the movements they are capable of are very limited: most motors are designed to perform simple linear movement; while in some cases, the helical micromotors can adapt axial rotation, but it's also used to trigger linear movement. Because of the improved deformability and added degrees of freedom, soft actuators can have more agile locomotion, such as bending and contraction; thus, well-designed soft robots can perform movements that resemble biological systems, such as walking, jumping, crawling, rolling, etc[224]. Even for those untethered soft robots, these advanced movements were also achieved[226, 227]. This flexible and intelligent movement not only enables them to tackle more challenging manipulations, but also provides potential tools to be leveraged as sensing mechanisms. On the other hand, actuation on soft robotics involves a variety of different methods that are typically safer and more biocompatible, such as pneumatic actuation, light actuation, thermal actuation, electrical actuation, and bio-hybrid actuation[214], based on the applied geometrical configuration and materials. For example, as a very popular actuation method, pneumatic actuation features fast response, controllable actuating force, and substantial strain.

However, the current development of soft robotics as sensors is still focused on physical sensings[217], such as proprioception[228–230], pressure/tactile sensing[231–233], and they are primarily used as feedback component for the closed-loop controlling strategy[225]. On the contrary, the utilization of soft robotics in bio- and chemical sensing is rather in its infancy. Cheemeng Tan et al functionalized a soft gripper with synthetic bacteria as a biosensing

soft robot[234] (Figure 10A). By integrating the genetically engineered E. coli., they created a hybrid bio-light-emitting diode-actuator structure that could allow chemical diffusion, prevent the escape of bacteria, and transduce the generated biological signal. The embedded chemosensitive bacteria can detect and respond to an external chemical signal (isopropyl β-D-1-thiogalactopryanoside, IPTG), using its genetic response (transcription of green fluorescence protein) to trigger robotic decision-making and actuation (object pick-up). In this example, the sensing function of soft robotics was expanded by adopting an existing biological modality. Meanwhile, there are numerous cases of soft bio- and chemical sensors, but they are mostly used as wearable electronic devices for the sensing and monitoring of human sweat or other bodily fluids[235–238]. In a recent review[239], the authors pointed out the fascinating prospect of combing electronic skin and machine learning for the next-generation of intelligent soft robots - as soft robotics offer inherent advantages to be coupled with wearable devices. In this regard, we believe there is immeasurable potential of soft robotics in bio- and chemical sensing, and this field is sure to proliferate in the coming future. Material chemists have significantly contributed to the development of soft robotics, and analytical chemists should not miss out on this opportunity.

So, what is the next step? The effective functionalization of high-performance biological and chemical probes is inevitable, because compared to physical parameters, the bio- and chemical analytes are less robust and detection conditions are more demanding[240]. The compatibility of chemical probes on the flexible interface should be investigated. How to translate the information of bio- and chemical analytes into the soft movement (such as bending and contraction) is also an important and promising task of the applied interface. At the same time, size matters. The ability to tackle minute volume of sample is extremely important for biological, chemical and clinical research[241], but the working size of current soft robotics are generally from several centimeters to several meters, which is difficult to be coupled to most analytical instruments (such as microscopes). Downsizing the scale of soft robots is a key challenge to the current fabrication methods, with potentially higher cost and more complicated procedures. However, this also brings opportunities in the innovation from materials, design, manufacturing to applications[242, 243]. In 2016, the Nelson group developed a magnetic soft micromachine by origami-inspired self-assembly[244] (Figure 10B). Using thermally responsive layered hydrogels, the micromachine can have different magnetic anisotropy and undergo programmable and reversible shape transformation. In this way, with different morphologies, different corresponding propulsion strategies could be applied, which is difficult to achieve in rigid robotics. Recently, John Rogers's group fabricated a terrestrial robot at submillimeter scale (~ 500 μm)[245]. They used techniques in semiconducting to fabricate 3D geometries of the robot from multilayer lithographically designed 2D structures. Polyimide film was used as static skeleton for support, and nitinol shape memory alloy was used as a collection of dynamic chemical joints; they were buckled by a silica shell and then transferred to a pre-stretched PDMS film to obtain the 3D structure. Altogether, this spider-like robot can perform walking, turning, jumping, and linear/curvilinear crawling. Typically, the direct coupling of microscale living organisms, namely biohybrid system, is a very attractive and promising strategy for the fabrication of microscale soft robotics[246]. Leveraging the well-evolved and inherent soft structures from nature can greatly accelerate the process toward effective micro- and nanoscale soft robotics,

while the concern of safety and biocompatibility can be easier to circumvent[247, 248]. These cases have proven that, even though there is a huge gap between the current macroscale and miniaturized soft robotics, this field can be a game-changer if it combines the advantages from both micro-/nanorobotics and soft robotics[249].

6. Conclusions

In this review, we focus on the progress of the emerging micro-/nanorobotics in the field of bio- and chemical sensing. First, the propulsion methods are summarized, including chemical propulsion, acoustic propulsion, and light-driven propulsion. Micro-/nanorobotics have exhibited several advantages for various biomedical applications, and the fields of bio- and chemical sensing have also benefitted from their inclusion, so next, noticeable advances in micro/nanorobotics for bio- and chemical sensing are concluded and discussed according to the different sensing strategies: 1) motion-based sensing; 2) optical sensing; and 3) electrochemical sensing. After that, more broad applications based on sensing, including target transport and delivery, pollutant removal, and swarm behaviors are also introduced. However, despite the widely recognized promises, the drawbacks and limitations of micro-/nanorobotics in these applications are also depicted, such as high cost as well as low compatibility at times. Another field of robotics, soft robotics, has proven to be an outstanding candidate for a broad range of biomedical applications, and its unique characteristics have the potential to be promising solutions to the challenges normally encountered by micro-/nanorobotics. In the area of sensing, even though soft robotics had actively participated in the sensing devices for healthcare purposes, it's still underrepresented in bio- and chemical sensing. Compared to physical parameters, the information from bio- and chemical analysis is more abundant and prompt for personal healthcare and advanced disease research[250]. Therefore, it is fascinating to envision a new field that applies soft robotics in bio- and chemical sensing, and we hope this review can stimulate wide awareness and inspire the exciting research of tomorrow.

Acknowledgements

References

1. Feynman R, in Feynman and computation, CRC Press, 2018, pp. 63–76.

2. Wang J, Dong Y, Ma P, Wang Y, Zhang F, Cai B, Chen P and Liu B-F, Advanced Materials, 2022, 34, 2201051.

3. Hu Y, Liu W and Sun Y, Advanced Functional Materials, 2022, 32, 2109181.

4. Wang J, Xiong Z, Zheng J, Zhan X and Tang J, Accounts of chemical research, 2018, 51, 1957–1965. [PubMed: 30179455]

5. Medina-Sánchez M, Xu H and Schmidt OG, Therapeutic delivery, 2018, 9, 303–316. [PubMed: 29540126]

6. Ye H, Wang Y, Xu D, Liu X, Liu S and Ma X, Applied Materials Today, 2021, 23, 101007.

7. Kong L, Guan J and Pumera M, Current Opinion in Electrochemistry, 2018, 10, 174–182.

8. Choi H, Yi J, Cho SH and Hahn SK, Biomaterials, 2021, 279, 121201. [PubMed: 34715638]

9. Kim K, Guo J, Liang Z and Fan D, Advanced Functional Materials, 2018, 28, 1705867.

10. Whitesides GM, Angewandte Chemie International Edition, 2018, 57, 4258–4273. [PubMed: 29517838]

11. Ashuri T, Armani A, Jalilzadeh Hamidi R, Reasnor T, Ahmadi S and Iqbal K, Biomedical Engineering Letters, 2020, 10, 369–385. [PubMed: 32864173]

12. Cianchetti M, Laschi C, Menciassi A and Dario P, Nature Reviews Materials, 2018, 3, 143–153.

13. Halder A and Sun Y, Biosensors and Bioelectronics, 2019, 139, 111334. [PubMed: 31128479]

14. Ceylan H, Giltinan J, Kozielski K and Sitti M, Lab on a Chip, 2017, 17, 1705–1724. [PubMed: 28480466]

15. Zhou L, Wei Y, Zhang H, Zhao Q, Zhao Z, Guo Y, Zhu S, Fu H and Cai W, ACS Applied Nano Materials, 2022, 5, 18469–18478.

16. Wang W, Duan W, Ahmed S, Mallouk TE and Sen A, Nano Today, 2013, 8, 531–554.

17. Safdar M, Khan SU and Jänis J, Advanced Materials, 2018, 30, 1703660.

18. Moran JL and Posner JD, Physics today, 2019, 72, 44–52.

19. Howse JR, Jones RA, Ryan AJ, Gough T, Vafabakhsh R and Golestanian R, Physical review letters, 2007, 99, 048102. [PubMed: 17678409]

20. Lee T-C, Alarcón-Correa M, Miksch C, Hahn K, Gibbs JG and Fischer P, Nano letters, 2014, 14, 2407–2412. [PubMed: 24707952]

21. Das SS, Erez S, Karshalev E, Wu Y, Wang J and Yossifon G, ACS Applied Materials & Interfaces, 2022, 14, 30290–30298. [PubMed: 35748802]

22. Liu L, Bai T, Chi Q, Wang Z, Xu S, Liu Q and Wang Q, Micromachines, 2017, 8, 267. [PubMed: 30400455]

23. Wang B, Kostarelos K, Nelson BJ and Zhang L, Advanced Materials, 2021, 33, 2002047.

24. Li Y, Mou F, Chen C, You M, Yin Y, Xu L and Guan J, RSC advances, 2016, 6, 10697–10703.

25. Magdanz V, Stoychev G, Ionov L, Sanchez S and Schmidt OG, Angewandte Chemie, 2014, 126, 2711–2715.

26. Wu Z, Lin X, Wu Y, Si T, Sun J and He Q, Acs Nano, 2014, 8, 6097–6105. [PubMed: 24806430]

27. Demirbuken SE, Karaca GY, Kaya HK, Oksuz L, Garipcan B, Oksuz AU and Kuralay F, Materials Today Chemistry, 2022, 26, 101172.

28. Zhou H, Mayorga-Martinez CC, Pané S, Zhang L and Pumera M, Chemical Reviews, 2021, 121, 4999–5041. [PubMed: 33787235]

29. Purcell EM, American journal of physics, 1977, 45, 3–11.

30. Ceylan H, Dogan NO, Yasa IC, Musaoglu MN, Kulali ZU and Sitti M, Science Advances, 2021, 7, eabh0273. [PubMed: 34516907]

31. Wang Z, Xu Z, Zhu B, Zhang Y, Lin J, Wu Y and Wu D, Nanotechnology, 2022, 33, 152001.

32. Yu S, Sun Z, Zhang Z, Sun H, Liu L, Wang W, Li M, Zhao Q and Li T, Frontiers in Bioengineering and Biotechnology, 2021, 9.

33. Wang Q, Yu J, Yuan K, Yang L, Jin D and Zhang L, Applied Materials Today, 2020, 18, 100489.

34. Jang B, Gutman E, Stucki N, Seitz BF, Wendel-García PD, Newton T, Pokki J, Ergeneman O, Pané S and Or Y, Nano letters, 2015, 15, 4829–4833. [PubMed: 26029795]

35. Li T, Li J, Zhang H, Chang X, Song W, Hu Y, Shao G, Sandraz E, Zhang G and Li L, Small, 2016, 12, 6098–6105. [PubMed: 27600373]

36. Obara K, Kageyama Y and Takeda S, Small, 2022, 18, 2105302.

37. Qiu T, Lee T-C, Mark AG, Morozov KI, Münster R, Mierka O, Turek S, Leshansky AM and Fischer P, Nature communications, 2014, 5, 5119.

38. Nitschke T, Stenhammar J and Wittkowski R, Nanoscale Advances, 2022, 4, 2844–2856. [PubMed: 36132012]

39. Ren L, Wang W and Mallouk TE, Accounts of chemical research, 2018, 51, 1948–1956. [PubMed: 30079719]

40. Valdez-Garduño M, Leal-Estrada M, Oliveros-Mata ES, Sandoval-Bojorquez DI, Soto F, Wang J and Garcia-Gradilla V, Advanced Functional Materials, 2020, 30, 2004043.

41. Collis JF, Chakraborty D and Sader JE, Journal of Fluid Mechanics, 2017, 825, 29–48.

42. Gao Y, Xiong Z, Wang J, Tang J and Li D, Nano Research, 2022, 15, 5355–5375.

43. Li J, He X, Jiang H, Xing Y, Fu B and Hu C, ACS Applied Materials & Interfaces, 2022, 14, 36027–36037. [PubMed: 35916408]

44. Zhang Q, Dong R, Wu Y, Gao W, He Z and Ren B, ACS Applied Materials & Interfaces, 2017, 9, 4674–4683. [PubMed: 28097861]

45. Lin X, Si T, Wu Z and He Q, Physical Chemistry Chemical Physics, 2017, 19, 23606–23613. [PubMed: 28530758]

46. Xu L, Mou F, Gong H, Luo M and Guan J, Chemical Society Reviews, 2017, 46, 6905–6926. [PubMed: 28949354]

47. Wu J, Ma S, Li M, Hu X, Jiao N, Tung S and Liu L, ACS Applied Materials & Interfaces, 2021, 13, 31514–31526. [PubMed: 34213305]

48. Xing Y, Zhou M, Xu T, Tang S, Fu Y, Du X, Su L, Wen Y, Zhang X and Ma T, Angewandte Chemie International Edition, 2020, 59, 14368–14372. [PubMed: 32506778]

49. Karaca GY, Kuralay F, Uygun E, Ozaltin K, Demirbuken SE, Garipcan B, Oksuz L and Oksuz AU, ACS Applied Nano Materials, 2021, 4, 3377–3388.

50. Shao J, Cao S, Che H, De Martino MT, Wu H, Abdelmohsen LK and van Hest JC, Journal of the American Chemical Society, 2022, 144, 11246–11252. [PubMed: 35700477]

51. Yuan K, Jurado-Sánchez B and Escarpa A, Angewandte Chemie International Edition, 2021, 60, 4915–4924. [PubMed: 33216439]

52. del Barrio J and Sánchez-Somolinos C, Advanced Optical Materials, 2019, 7, 1900598.

53. Medina-Sánchez M, Magdanz V, Guix M, Fomin VM and Schmidt OG, Advanced Functional Materials, 2018, 28, 1707228.

54. Wang H, Song X, Xiong J and Cheang UK, Polymers, 2022, 14, 5509. [PubMed: 36559876]

55. Tan L and Cappelleri DJ, IEEE Robotics and Automation Letters, 2023, 8, 1723–1730.

56. Iacovacci V, Blanc A, Huang H, Ricotti L, Schibli R, Menciassi A, Behe M, Pané S and Nelson BJ, Small, 2019, 15, 1900709.

57. Mu X, Zhong Y, Jiang T and Cheang UK, Materials Advances, 2021, 2, 3871–3880.

58. Li Z, Xie Z, Lu H, Wang Y and Liu Y, ChemistryOpen, 2021, 10, 861–866. [PubMed: 34346565]

59. Lu X, Ou H, Wei Y, Ding X, Wang X, Zhao C, Bao J and Liu W, Sensors and Actuators B: Chemical, 2022, 372, 132667.

60. Ji F, Li T, Yu S, Wu Z and Zhang L, ACS Nano, 2021, 15, 5118–5128. [PubMed: 33687190]

61. Ye J, Wilson DA, Tu Y and Peng F, Advanced Materials Technologies, 2020, 5, 2000435.

62. Otuka AJG, Corrêa DS, Fontana CR and Mendonça CR, Materials Science and Engineering: C, 2014, 35, 185–189. [PubMed: 24411367]

63. Li J and Pumera M, Chemical Society Reviews, 2021, 50, 2794–2838. [PubMed: 33470252]

64. Liu Z, Li M, Dong X, Ren Z, Hu W and Sitti M, Nature Communications, 2022, 13, 2016.

65. Alsharhan AT, Young OM, Xu X, Stair AJ and Sochol RD, Journal of Micromechanics and Microengineering, 2021, 31, 044001.

66. Zhao Y, Ye D, Wang G-C and Lu T-M, 2003.

67. Dasgupta D, Peddi S, Saini DK and Ghosh A, Advanced Healthcare Materials, 2022, 11, 2200232.

68. Ghosh S and Ghosh A, Journal of Micro-Bio Robotics, 2020, 16, 33–42.

69. Rivas D, Mallick S, Sokolich M and Das S, 2022.

70. Cohen L and Walt DR, Chemical reviews, 2018, 119, 293–321. [PubMed: 30152694]

71. Pereiro I, Fomitcheva-Khartchenko A and Kaigala GV, Analytical Chemistry, 2020, 92, 10187–10195. [PubMed: 32515583]

72. Lafleur JP, Jönsson A, Senkbeil S and Kutter JP, Biosensors and Bioelectronics, 2016, 76, 213–233. [PubMed: 26318580]

73. Squires TM, Messinger RJ and Manalis SR, Nature biotechnology, 2008, 26, 417–426.

74. Lopez M and Graham MD, Physics of Fluids, 2008, 20, 053304.

75. Atencia J and Beebe DJ, Nature, 2005, 437, 648–655. [PubMed: 16193039]

76. Mocanu D, Kolesnychenko A, Aarts S, Troost-Dejong A, Pierik A, Vossenaar E and Stapert H, Journal of Biotechnology, 2009, 139, 179–185. [PubMed: 18984014]

77. Pereiro I, Fomitcheva Khartchenko A, Lovchik RD and Kaigala GV, Angewandte Chemie International Edition, 2021, 60, 20935–20942. [PubMed: 34296491]

78. Yoon SK, Fichtl GW and Kenis PJA, Lab on a Chip, 2006, 6, 1516–1524. [PubMed: 17203155]

79. Garcia-Guirado J, Rica RA, Ortega J, Medina J, Sanz V, Ruiz-Reina E and Quidant R, ACS Photonics, 2018, 5, 3673–3679.

80. Marschewski J, Jung S, Ruch P, Prasad N, Mazzotti S, Michel B and Poulikakos D, Lab on a Chip, 2015, 15, 1923–1933. [PubMed: 25737365]

81. Zhang P, Zhou X, He M, Shang Y, Tetlow AL, Godwin AK and Zeng Y, Nature Biomedical Engineering, 2019, 3, 438–451.

82. Zhang P, Zhou X and Zeng Y, Chemical Science, 2019, 10, 5495–5504. [PubMed: 31293733]

83. Zhang P, Wu X, Gardashova G, Yang Y, Zhang Y, Xu L and Zeng Y, Science translational medicine, 2020, 12, eaaz2878. [PubMed: 32522804]

84. Paratore F, Zeidman Kalman T, Rosenfeld T, Kaigala GV and Bercovici M, Analytical Chemistry, 2017, 89, 7373–7381. [PubMed: 28459549]

85. Bercovici M, Han CM, Liao JC and Santiago JG, Proceedings of the National Academy of Sciences, 2012, 109, 11127–11132.

86. Renaudin A, Chabot V, Grondin E, Aimez V and Charette PG, Lab on a Chip, 2010, 10, 111–115. [PubMed: 20024058]

87. Agostini M, Lunardelli F, Gagliardi M, Miranda A, Lamanna L, Luminare AG, Gambineri F, Lai M, Pistello M and Cecchini M, Advanced Functional Materials, 2022, 32, 2201958.

88. Zhou M, Gao D, Yang Z, Zhou C, Tan Y, Wang W and Jiang Y, Talanta, 2021, 222, 121480. [PubMed: 33167205]

89. Emaminejad S, Javanmard M, Gupta C, Chang S, Davis RW and Howe RT, Proceedings of the National Academy of Sciences, 2015, 112, 1995–1999.

90. Yan H, Wen Y, Han S, Hughes SJ and Zeng Y, bioRxiv, 2022, DOI: 10.1101/2022.05.01.490215, 2022.2005.2001.490215.

91. Katira P and Hess H, Nano Letters, 2010, 10, 567–572. [PubMed: 20055432]

92. Karshalev E, Esteban-Fernández de Ávila B and Wang J, Journal of the American Chemical Society, 2018, 140, 3810–3820. [PubMed: 29470916]

93. Zizzari A, Cesaria M, Bianco M, del Mercato LL, Carraro M, Bonchio M, Rella R and Arima V, Chemical Engineering Journal, 2020, 391, 123572.

94. Kagan D, Calvo-Marzal P, Balasubramanian S, Sattayasamitsathit S, Manesh KM, Flechsig G-U and Wang J, Journal of the American Chemical Society, 2009, 131, 12082–12083. [PubMed: 19670862]

95. Moo JGS, Wang H, Zhao G and Pumera M, Chemistry – A European Journal, 2014, 20, 4292–4296. [PubMed: 24652757]

96. Orozco J, García-Gradilla V, D'Agostino M, Gao W, Cortes A and Wang J, ACS nano, 2013, 7, 818–824. [PubMed: 23234238]

97. Maric T, Mayorga-Martinez CC, Nasir MZM and Pumera M, Advanced Materials Technologies, 2019, 4, 1800502.

98. Su Y, Ge Y, Liu L, Zhang L, Liu M, Sun Y, Zhang H and Dong B, ACS Applied Materials & Interfaces, 2016, 8, 4250–4257. [PubMed: 26815003]

99. Wu J, Balasubramanian S, Kagan D, Manesh KM, Campuzano S and Wang J, Nature Communications, 2010, 1, 36.

100. Wang J and Gao W, ACS Nano, 2012, 6, 5745–5751. [PubMed: 22770233]

101. Van Nguyen K and Minteer SD, Chemical Communications, 2015, 51, 4782–4784. [PubMed: 25697823]

102. Fu S, Zhang X, Xie Y, Wu J and Ju H, Nanoscale, 2017, 9, 9026–9033. [PubMed: 28639653]

103. Zhang X, Chen C, Wu J and Ju H, ACS applied materials & interfaces, 2019, 11, 13581–13588. [PubMed: 30888785]

104. Luo M, Li S, Wan J, Yang C, Chen B and Guan J, Langmuir, 2020, 36.

105. Li M, Zhang H, Liu M and Dong B, Journal of Materials Chemistry C, 2017, 5, 4400–4407.

106. Molinero-Fernández Á, Jodra A, Moreno-Guzmán M, López MÁ and Escarpa A, Chemistry – A European Journal, 2018, 24, 7172–7176. [PubMed: 29469987]

107. Jurado-Sánchez B, Pacheco M, Rojo J and Escarpa A, Angewandte Chemie International Edition, 2017, 56, 6957–6961. [PubMed: 28504463]

108. Soto F, Wang J, Ahmed R and Demirci U, Advanced Science, 2020, 7, 2002203. [PubMed: 33173743]

109. Wang L, Meng Z, Chen Y and Zheng Y, Advanced Intelligent Systems, 2021, 3, 2000267.

110. Pal M, Somalwar N, Singh A, Bhat R, Eswarappa SM, Saini DK and Ghosh A, Advanced Materials, 2018, 30, 1800429.

111. Bonakdar N, Gerum R, Kuhn M, Spörrer M, Lippert A, Schneider W, Aifantis KE and Fabry B, Nature Materials, 2016, 15, 1090–1094. [PubMed: 27376682]

112. Wang X, Ho C, Tsatskis Y, Law J, Zhang Z, Zhu M, Dai C, Wang F, Tan M, Hopyan S, McNeill H and Sun Y, Science Robotics, 2019, 4, eaav6180. [PubMed: 33137746]

113. Berret J-F, Nature communications, 2016, 7, 1–9.

114. Pal M, Dasgupta D, Somalwar N, Vr R, Tiwari M, Teja D, Narayana SM, Katke A, Rs J, Bhat R, Saini DK and Ghosh A, Journal of Physics: Condensed Matter, 2020, 32, 224001. [PubMed: 31978922]

115. Wang L, Li T, Li L, Wang J, Song W and Zhang G, ECS Journal of Solid State Science and Technology, 2015, 4, S3020.

116. Draz MS, Kochehbyoki KM, Vasan A, Battalapalli D, Sreeram A, Kanakasabapathy MK, Kallakuri S, Tsibris A, Kuritzkes DR and Shafiee H, Nature Communications, 2018, 9, 4282.

117. Draz MS, Lakshminaraasimulu NK, Krishnakumar S, Battalapalli D, Vasan A, Kanakasabapathy MK, Sreeram A, Kallakuri S, Thirumalaraju P, Li Y, Hua S, Yu XG, Kuritzkes DR and Shafiee H, ACS Nano, 2018, 12, 5709–5718. [PubMed: 29767504]

118. Yuan K, Cuntín-Abal C, Jurado-Sánchez B and Escarpa A, Analytical Chemistry, 2021, 93, 16385–16392. [PubMed: 34806352]

119. Yang M, Guo X, Mou F and Guan J, Chemical Reviews, 2022, DOI: 10.1021/acs.chemrev.2c00062.

120. Jurado-Sánchez B, Escarpa A and Wang J, Chemical Communications, 2015, 51, 14088–14091. [PubMed: 26252562]

121. Singh VV, Kaufmann K, Orozco J, Li J, Galarnyk M, Arya G and Wang J, Chemical Communications, 2015, 51, 11190–11193. [PubMed: 26072740]

122. Villa K, Manzanares Palenzuela CL, Sofer Z. k., Mat jková S and Pumera M, ACS nano, 2018, 12, 12482–12491. [PubMed: 30495923]

123. Yang W, Li J, Xu Z, Yang J, Liu Y and Liu L, Journal of Materials Chemistry C, 2019, 7, 10297–10308.

124. Molinero-Fernández A. g., Moreno-Guzman M, López M. A. n. and Escarpa A, Analytical chemistry, 2017, 89, 10850–10857. [PubMed: 28889736]

125. Pacheco M, Jurado-Sánchez B and Escarpa A, Analytical chemistry, 2018, 90, 2912–2917. [PubMed: 29376315]

126. Wang K, Wang W, Pan S, Fu Y, Dong B and Wang H, Applied Materials Today, 2020, 19, 100550.

127. Liu M, Sun Y, Wang T, Ye Z, Zhang H, Dong B and Li CY, Journal of Materials Chemistry C, 2016, 4, 5945–5952.

128. Esteban-Fernández de Ávila B, Martín A, Soto F, Lopez-Ramirez MA, Campuzano S, Vasquez-Machado GM, Gao W, Zhang L and Wang J, Acs Nano, 2015, 9, 6756–6764. [PubMed: 26035455]

129. Esteban-Fernández de Ávila B, Lopez-Ramirez MA, Báez DF, Jodra A, Singh VV, Kaufmann K and Wang J, ACS sensors, 2016, 1, 217–221.

130. Singh VV, Kaufmann K, de Ávila BEF, Karshalev E and Wang J, Advanced Functional Materials, 2016, 26, 6270–6278.

131. Pacheco M, de la Asunción-Nadal V, Jurado-Sánchez B and Escarpa A, Biosensors and Bioelectronics, 2020, 165, 112286. [PubMed: 32729468]

132. la Asunción-Nadal V. c. d., Pacheco M, Jurado-Sanchez B and Escarpa A, Analytical Chemistry, 2020, 92, 9188–9193. [PubMed: 32521995]

133. Zhao L, Xie S, Liu Y, Liu Q, Song X and Li X, Nanoscale, 2019, 11, 17831–17840. [PubMed: 31552986]

134. Zhao L, Liu Y, Xie S, Ran P, Wei J, Liu Q and Li X, Chemical Engineering Journal, 2020, 382, 123041.

135. Qin F, Wu J, Fu D, Feng Y, Gao C, Xie D, Fu S, Liu S, Wilson DA and Peng F, Applied Materials Today, 2022, 27, 101456.

136. Zhang Y, Yang F, Wei W, Wang Y, Yang S, Li J, Xing Y, Zhou L, Dai W and Dong H, ACS nano, 2022, 16, 5587–5596. [PubMed: 35357821]

137. Yuan K, de la Asunción-Nadal V, Cuntín-Abal C, Jurado-Sánchez B and Escarpa A, Lab on a Chip, 2022, 22, 928–935. [PubMed: 34994753]

138. García M, Orozco J, Guix M, Gao W, Sattayasamitsathit S, Escarpa A, Merkoçi A and Wang J, Nanoscale, 2013, 5, 1325–1331. [PubMed: 23123833]

139. Morales-Narváez E, Guix M, Medina-Sánchez M, Mayorga-Martinez CC and Merkoçi A, Small, 2014, 10, 2542–2548. [PubMed: 24634101]

140. Yu X, Li Y, Wu J and Ju H, Analytical Chemistry, 2014, 86, 4501–4507. [PubMed: 24731140]

141. Vilela D, Orozco J, Cheng G, Sattayasamitsathit S, Galarnyk M, Kan C, Wang J and Escarpa A, Lab on a Chip, 2014, 14, 3505–3509. [PubMed: 25017813]

142. de Ávila BE-F, Zhao M, Campuzano S, Ricci F, Pingarrón JM, Mascini M and Wang J, Talanta, 2017, 167, 651–657. [PubMed: 28340774]

143. Wang Y, Liu X, Chen C, Chen Y, Li Y, Ye H, Wang B, Chen H, Guo J and Ma X, ACS Nano, 2022, 16, 180–191. [PubMed: 35015504]

144. Molinero-Fernández Á, Moreno-Guzmán M, Arruza L, López MÁ and Escarpa A, ACS Sensors, 2020, 5, 1336–1344. [PubMed: 32204587]

145. Molinero-Fernández A. g., López M. A. n. and Escarpa A, Analytical chemistry, 2020, 92, 5048–5054. [PubMed: 32154703]

146. Lu C, Liu X, Li Y, Yu F, Tang L, Hu Y and Ying Y, ACS Applied Materials & Interfaces, 2015, 7, 15395–15402. [PubMed: 26110779]

147. María-Hormigos R, Jurado-Sánchez B and Escarpa A, Analytical Chemistry, 2018, 90, 9830–9837. [PubMed: 29906091]

148. Sharma B, Frontiera RR, Henry A-I, Ringe E and Van Duyne RP, Materials Today, 2012, 15, 16–25.

149. Han D, Fang Y, Du D, Huang G, Qiu T and Mei Y, Nanoscale, 2016, 8, 9141–9145. [PubMed: 27092767]

150. Wang Y, Zhou C, Wang W, Xu D, Zeng F, Zhan C, Gu J, Li M, Zhao W and Zhang J, Angewandte Chemie, 2018, 130, 13294–13297.

151. Novotný F, Plutnar J and Pumera M, Advanced Functional Materials, 2019, 29, 1903041.

152. Fan X, Hao Q, Li M, Zhang X, Yang X, Mei Y and Qiu T, ACS applied materials & interfaces, 2020, 12, 28783–28791. [PubMed: 32469196]

153. Liu X, Chen W, Zhao D, Liu X, Wang Y, Chen Y and Ma X, ACS nano, 2022, 16, 10354–10363. [PubMed: 35816232]

154. Privett BJ, Shin JH and Schoenfisch MH, Analytical Chemistry, 2010, 82, 4723–4741. [PubMed: 20476724]

155. Cinti S, Valdés-Ramírez G, Gao W, Li J, Palleschi G and Wang J, Chemical Communications, 2015, 51, 8668–8671. [PubMed: 25908115]

156. Rojas D, Jurado-Sánchez B and Escarpa A, Analytical chemistry, 2016, 88, 4153–4160. [PubMed: 26938969]

157. Kong L, Rohaizad N, Nasir MZM, Guan J and Pumera M, Analytical chemistry, 2019, 91, 5660–5666. [PubMed: 30986039]

158. Moo JGS, Zhao G and Pumera M, The Journal of Physical Chemistry C, 2014, 118, 29896–29902.

159. Moo JGS and Pumera M, ACS Sensors, 2016, 1, 949–957.

160. Khezri B, Sheng Moo JG, Song P, Fisher AC and Pumera M, RSC Advances, 2016, 6, 99977–99982.

161. Wang Q, Tang X, Lv R, Tan K, Zhao Z, Wan M and Mao C, Chemical Engineering Journal, 2022, 430, 132665.

162. Gao W, de Ávila BE-F, Zhang L and Wang J, Advanced Drug Delivery Reviews, 2018, 125, 94–101. [PubMed: 28893551]

163. Campuzano S, Orozco J, Kagan D, Guix M, Gao W, Sattayasamitsathit S, Claussen JC, Merkoçi A and Wang J, Nano letters, 2012, 12, 396–401. [PubMed: 22136558]

164. Orozco J, Campuzano S, Kagan D, Zhou M, Gao W and Wang J, Analytical chemistry, 2011, 83, 7962–7969. [PubMed: 21888314]

165. Kagan D, Campuzano S, Balasubramanian S, Kuralay F, Flechsig G-U and Wang J, Nano letters, 2011, 11, 2083–2087. [PubMed: 21491941]

166. Balasubramanian S, Kagan D, Jack Hu CM, Campuzano S, Lobo-Castañon MJ, Lim N, Kang DY, Zimmerman M, Zhang L and Wang J, Angewandte Chemie, 2011, 123, 4247–4250.

167. Orozco J, Cortés A, Cheng G, Sattayasamitsathit S, Gao W, Feng X, Shen Y and Wang J, Journal of the American Chemical Society, 2013, 135, 5336–5339. [PubMed: 23530475]

168. Huang C and Shen X, Chemical Communications, 2014, 50, 2646–2649. [PubMed: 24469062]

169. Li J, Angsantikul P, Liu W, Esteban-Fernández de Ávila B, Chang X, Sandraz E, Liang Y, Zhu S, Zhang Y and Chen C, Advanced Materials, 2018, 30, 1704800.

170. Esteban-Fernández de Ávila B, Angsantikul P, Ramírez-Herrera DE, Soto F, Teymourian H, Dehaini D, Chen Y, Zhang L and Wang J, Science Robotics, 2018, 3, eaat0485. [PubMed: 33141704]

171. Qiu F, Fujita S, Mhanna R, Zhang L, Simona BR and Nelson BJ, Advanced Functional Materials, 2015, 25, 1666–1671.

172. Kadiri VM, Bussi C, Holle AW, Son K, Kwon H, Schütz G, Gutierrez MG and Fischer P, Advanced Materials, 2020, 32, 2001114.

173. Wang J, Liu X, Qi Y, Liu Z, Cai Y and Dong R, Chemical Engineering Journal, 2021, 416, 129091.

174. Zhang F, Zhuang J, de Ávila B. Esteban Fernández, Tang S, Zhang Q, Fang RH, Zhang L and Wang J, ACS Nano, 2019, 13, 11996–12005. [PubMed: 31556988]

175. Aziz A, Pane S, Iacovacci V, Koukourakis N, Czarske J. r., Menciassi A, Medina-Sánchez M and Schmidt OG, ACS nano, 2020, 14, 10865–10893. [PubMed: 32869971]

176. Xie L, Pang X, Yan X, Dai Q, Lin H, Ye J, Cheng Y, Zhao Q, Ma X, Zhang X, Liu G and Chen X, ACS Nano, 2020, 14, 2880–2893. [PubMed: 32125820]

177. Yan X, Zhou Q, Vincent M, Deng Y, Yu J, Xu J, Xu T, Tang T, Bian L and Wang Y-XJ, Science robotics, 2017, 2, eaaq1155. [PubMed: 33157904]

178. You M, Chen C, Xu L, Mou F and Guan J, Accounts of Chemical Research, 2018, 51, 3006–3014. [PubMed: 30444357]

179. Gwisai T, Mirkhani N, Christiansen MG, Nguyen TT, Ling V and Schuerle S, Science Robotics, 2022, 7, eabo0665. [PubMed: 36288270]

180. Wu Z, Li L, Yang Y, Hu P, Li Y, Yang S-Y, Wang LV and Gao W, Science Robotics, 2019, 4, eaax0613. [PubMed: 32632399]

181. Parmar J, Vilela D, Villa K, Wang J and Sánchez S, Journal of the American Chemical Society, 2018, 140, 9317–9331. [PubMed: 29969903]

182. Zhang Y, Yuan K and Zhang L, Advanced Materials Technologies, 2019, 4, 1800636.

183. Chang SH, Materials Today Sustainability, 2022, 19, 100196.

184. Villa K, Novotný F, Zelenka J, Browne MP, Ruml T. s. and Pumera M, ACS nano, 2019, 13, 8135–8145. [PubMed: 31283169]

185. Ying Y, Pourrahimi AM, Sofer Z, Mat jková S and Pumera M, ACS Nano, 2019, 13, 11477–11487. [PubMed: 31592633]

186. Guo Z, Liu J, Li Y, McDonald JA, Bin Zulkifli MY, Khan SJ, Xie L, Gu Z, Kong B and Liang K, Chemical Communications, 2020, 56, 14837–14840. [PubMed: 33174874]

187. Liang C, Zhan C, Zeng F, Xu D, Wang Y, Zhao W, Zhang J, Guo J, Feng H and Ma X, ACS applied materials & interfaces, 2018, 10, 35099–35107. [PubMed: 30246523]

188. Chen L, Yuan H, Chen S, Zheng C, Wu X, Li Z, Liang C, Dai P, Wang Q, Ma X and Yan X, ACS Applied Materials & Interfaces, 2021, 13, 31226–31235. [PubMed: 34176260]

189. Rubenstein M, Cornejo A and Nagpal R, Science, 2014, 345, 795–799. [PubMed: 25124435]

190. Wang Q and Zhang L, ACS Nano, 2021, 15, 149–174. [PubMed: 33417764]

191. Yang L, Yu J, Yang S, Wang B, Nelson BJ and Zhang L, IEEE Transactions on Robotics, 2022, 38, 1531–1551.

192. Jin D and Zhang L, Accounts of Chemical Research, 2022, 55, 98–109. [PubMed: 34931794]

193. Xie H, Sun M, Fan X, Lin Z, Chen W, Wang L, Dong L and He Q, Science Robotics, 2019, 4, eaav8006. [PubMed: 33137748]

194. Du X, Yu J, Jin D, Chiu PWY and Zhang L, ACS Nano, 2021, 15, 4429–4439. [PubMed: 33599480]

195. Yu J, Wang B, Du X, Wang Q and Zhang L, Nature Communications, 2018, 9, 3260.

196. Yu J, Jin D, Chan K-F, Wang Q, Yuan K and Zhang L, Nature Communications, 2019, 10, 5631.

197. Jin D, Yu J, Yuan K and Zhang L, ACS Nano, 2019, 13, 5999–6007. [PubMed: 31013052]

198. Dong Y, Wang L, Yuan K, Ji F, Gao J, Zhang Z, Du X, Tian Y, Wang Q and Zhang L, ACS Nano, 2021, 15, 5056–5067. [PubMed: 33634695]

199. Law J, Wang X, Luo M, Xin L, Du X, Dou W, Wang T, Shan G, Wang Y, Song P, Huang X, Yu J and Sun Y, Science Advances, 2022, 8, eabm5752. [PubMed: 35857830]

200. Mayorga-Martinez CC, Zelenka J, Klima K, Mayorga-Burrezo P, Hoang L, Ruml T and Pumera M, ACS Nano, 2022, 16, 8694–8703. [PubMed: 35507525]

201. Wang Q, Chan KF, Schweizer K, Du X, Jin D, Yu SCH, Nelson BJ and Zhang L, Science Advances, 2021, 7, eabe5914. [PubMed: 33637532]

202. Wang X, Hu C, Schurz L, De Marco C, Chen X, Pané S and Nelson BJ, ACS Nano, 2018, 12, 6210–6217. [PubMed: 29799724]

203. Mayorga-Martinez CC, Vyskoil J, Novotný F, Bednar P, Ruzek D, Alduhaishe O and Pumera M, Applied Materials Today, 2022, 26, 101337. [PubMed: 35018299]

204. Song S-J, Mayorga-Martinez CC, Vyskoil J, astorálová M, Ruml T and Pumera M, ACS Applied Materials & Interfaces, 2023, DOI: 10.1021/acsami.2c16592.

205. Teo WZ, Zboril R, Medrik I and Pumera M, Chemistry – A European Journal, 2016, 22, 4789–4793. [PubMed: 26845233]

206. de Ávila BE-F, Angsantikul P, Li J, Angel Lopez-Ramirez M, Ramírez-Herrera DE, Thamphiwatana S, Chen C, Delezuk J, Samakapiruk R, Ramez V, Obonyo M, Zhang L and Wang J, Nature Communications, 2017, 8, 272.

207. Choi H, Jeong SH, Kim TY, Yi J and Hahn SK, Bioactive Materials, 2022, 9, 54–62. [PubMed: 34820555]

208. Chen C, Karshalev E, Li J, Soto F, Castillo R, Campos I, Mou F, Guan J and Wang J, ACS Nano, 2016, 10, 10389–10396. [PubMed: 27783486]

209. Li C, Guo C, Fitzpatrick V, Ibrahim A, Zwierstra MJ, Hanna P, Lechtig A, Nazarian A, Lin SJ and Kaplan DL, Nature Reviews Materials, 2020, 5, 61–81.

210. Mestre R, Patiño T and Sánchez S, Wiley Interdisciplinary Reviews: Nanomedicine and Nanobiotechnology, 2021, 13, e1703. [PubMed: 33533200]

211. Fernández-Medina M, Ramos-Docampo MA, Hovorka O, Salgueiriño V and Städler B, Advanced Functional Materials, 2020, 30, 1908283.

212. Laschi C, Mazzolai B and Cianchetti M, Science Robotics, 2016, 1, eaah3690. [PubMed: 33157856]

213. Hines L, Petersen K, Lum GZ and Sitti M, Advanced materials, 2017, 29, 1603483.

214. Rich SI, Wood RJ and Majidi C, Nature Electronics, 2018, 1, 102–112.

215. Li M, Pal A, Aghakhani A, Pena-Francesch A and Sitti M, Nature Reviews Materials, 2022, 7, 235–249.

216. Pal A, Restrepo V, Goswami D and Martinez RV, Advanced Materials, 2021, 33, 2006939.

217. Wang H, Totaro M and Beccai L, Advanced Science, 2018, 5, 1800541. [PubMed: 30250796]

218. Sachyani Keneth E, Kamyshny A, Totaro M, Beccai L and Magdassi S, Advanced Materials, 2021, 33, 2003387.

219. Dong X, Luo X, Zhao H, Qiao C, Li J, Yi J, Yang L, Oropeza FJ, Hu TS, Xu Q and Zeng H, Soft Matter, 2022, 18, 7699–7734. [PubMed: 36205123]

220. Wehner M, Truby RL, Fitzgerald DJ, Mosadegh B, Whitesides GM, Lewis JA and Wood RJ, Nature, 2016, 536, 451–455. [PubMed: 27558065]

221. Jones TJ, Jambon-Puillet E, Marthelot J and Brun PT, Nature, 2021, 599, 229–233. [PubMed: 34759362]

222. Shintake J, Cacucciolo V, Floreano D and Shea H, Advanced Materials, 2018, 30, 1707035.

223. Hu W, Lum GZ, Mastrangeli M and Sitti M, Nature, 2018, 554, 81–85. [PubMed: 29364873]

224. Ng CSX, Tan MWM, Xu C, Yang Z, Lee PS and Lum GZ, Advanced Materials, 2021, 33, 2003558.

225. Wang J and Chortos A, Advanced Intelligent Systems, 2022, 4, 2100165.

226. Pantula A, Datta B, Shi Y, Wang M, Liu J, Deng S, Cowan NJ, Nguyen TD and Gracias DH, Science Robotics, 2022, 7, eadd2903. [PubMed: 36516274]

227. Kim Y, Yang Y, Zhang X, Li Z, Vázquez-Guardado A, Park I, Wang J, Efimov AI, Dou Z, Wang Y, Park J, Luan H, Ni X, Kim YS, Baek J, Park JJ, Xie Z, Zhao H, Gazzola M, Rogers JA and Bashir R, Science Robotics, 2023, 8, eadd1053. [PubMed: 36652505]

228. Soon RH, Yu L and Lim CT, Advanced Materials Technologies, 2020, 5, 2000150.

229. Luo M, Skorina EH, Tao W, Chen F, Ozel S, Sun Y and Onal CD, Soft Robotics, 2017, 4, 117–125. [PubMed: 29182091]

230. Helps T and Rossiter J, Soft Robotics, 2017, 5, 175–189. [PubMed: 29211627]

231. Sonar HA, Gerratt AP, Lacour SP and Paik J, Soft Robotics, 2019, 7, 22–29. [PubMed: 31549908]

232. Kumar N, Wirekoh J, Saba S, Riviere CN and Park Y-L, Soft Robotics, 2020, 8, 59–70. [PubMed: 32392453]

233. Ma B, Xu C, Cui L, Zhao C and Liu H, ACS Applied Materials & Interfaces, 2021, 13, 5574–5582. [PubMed: 33472372]

234. Justus KB, Hellebrekers T, Lewis DD, Wood A, Ingham C, Majidi C, LeDuc PR and Tan C, Science Robotics, 2019, 4, eaax0765. [PubMed: 33137770]

235. Zhu X, Ju Y, Chen J, Liu D and Liu H, ACS Sensors, 2018, 3, 1135–1141. [PubMed: 29767510]

236. Zhu X, Yuan S, Ju Y, Yang J, Zhao C and Liu H, Analytical Chemistry, 2019, 91, 10764–10771. [PubMed: 31361125]

237. Ma B, Chi J, Xu C, Ni Y, Zhao C and Liu H, Talanta, 2020, 212, 120786. [PubMed: 32113549]

238. Liu H and Zhao C, Current Opinion in Electrochemistry, 2020, 23, 42–46.

239. Shih B, Shah D, Li J, Thuruthel TG, Park Y-L, Iida F, Bao Z, Kramer-Bottiglio R and Tolley MT, Science Robotics, 2020, 5, eaaz9239. [PubMed: 33022628]

240. Yu Y, Li J, Solomon SA, Min J, Tu J, Guo W, Xu C, Song Y and Gao W, Science Robotics, 2022, 7, eabn0495. [PubMed: 35648844]

241. Cheng S, Li Y, Yan H, Wen Y, Zhou X, Friedman L and Zeng Y, Lab on a Chip, 2021, 21, 3219–3243. [PubMed: 34352059]

242. Hu C, Pané S and Nelson BJ, Annual Review of Control, Robotics, and Autonomous Systems, 2018, 1, 53–75.

243. Xia N, Zhu G, Wang X, Dong Y and Zhang L, Soft Matter, 2022, 18, 7464–7485. [PubMed: 36189642]

244. Huang H-W, Sakar MS, Petruska AJ, Pané S and Nelson BJ, Nature Communications, 2016, 7, 12263.

245. Han M, Guo X, Chen X, Liang C, Zhao H, Zhang Q, Bai W, Zhang F, Wei H and Wu C, Science Robotics, 2022, 7, eabn0602. [PubMed: 35613299]

246. Patino T, Mestre R and Sánchez S, Lab on a Chip, 2016, 16, 3626–3630. [PubMed: 27550016]

247. Appiah C, Arndt C, Siemsen K, Heitmann A, Staubitz A and Selhuber-Unkel C, Advanced Materials, 2019, 31, 1807747.

248. Lin Z, Jiang T and Shang J, Bio-Design and Manufacturing, 2022, 5, 107–132.

249. Sitti M, Nature Reviews Materials, 2018, 3, 74–75.

250. Kim J, Campbell AS, de Ávila BE-F and Wang J, Nature Biotechnology, 2019, 37, 389–406.
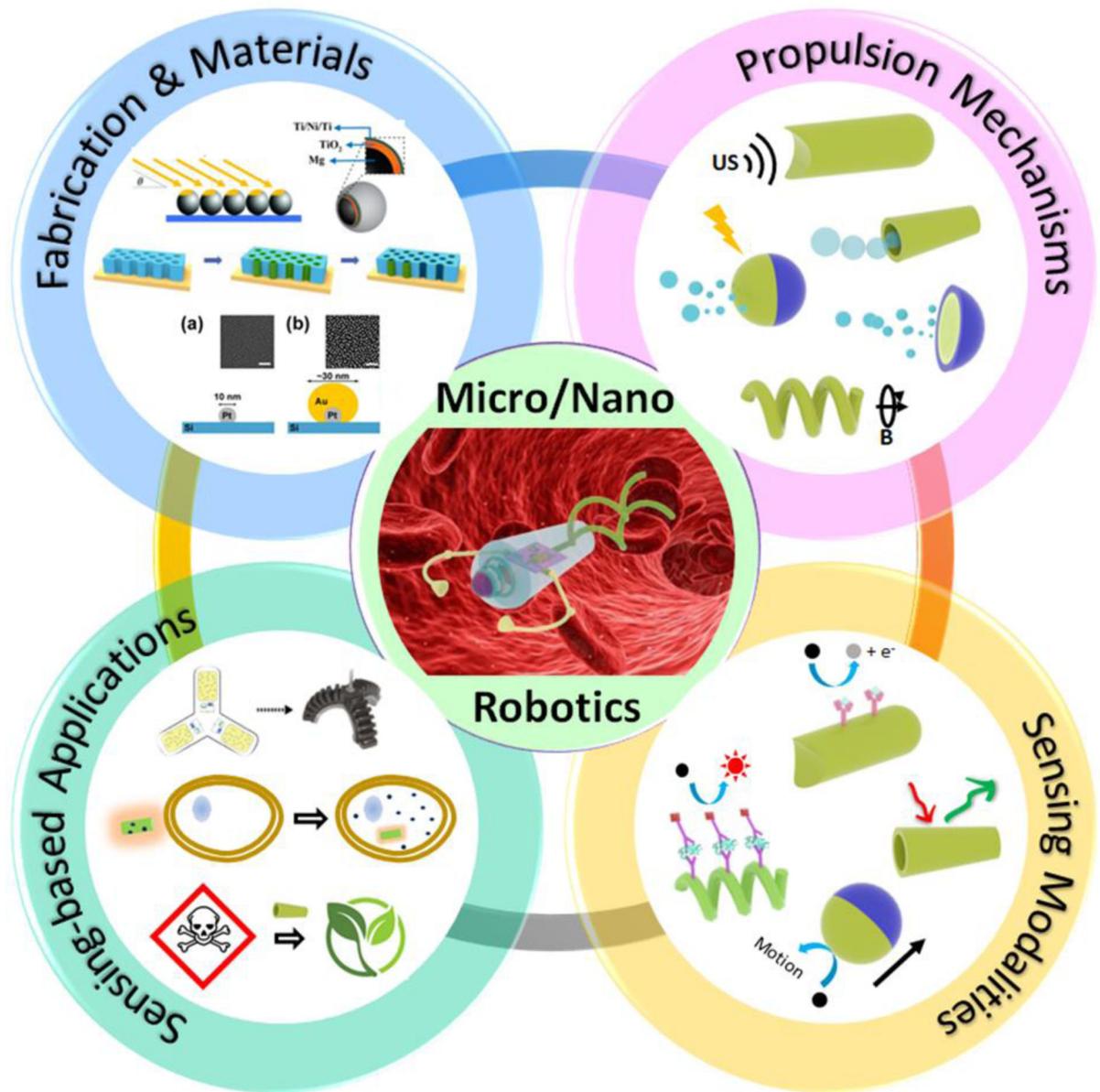
Figure 1.
Micro-/nanorobotics for sensing and sensing-based applications.
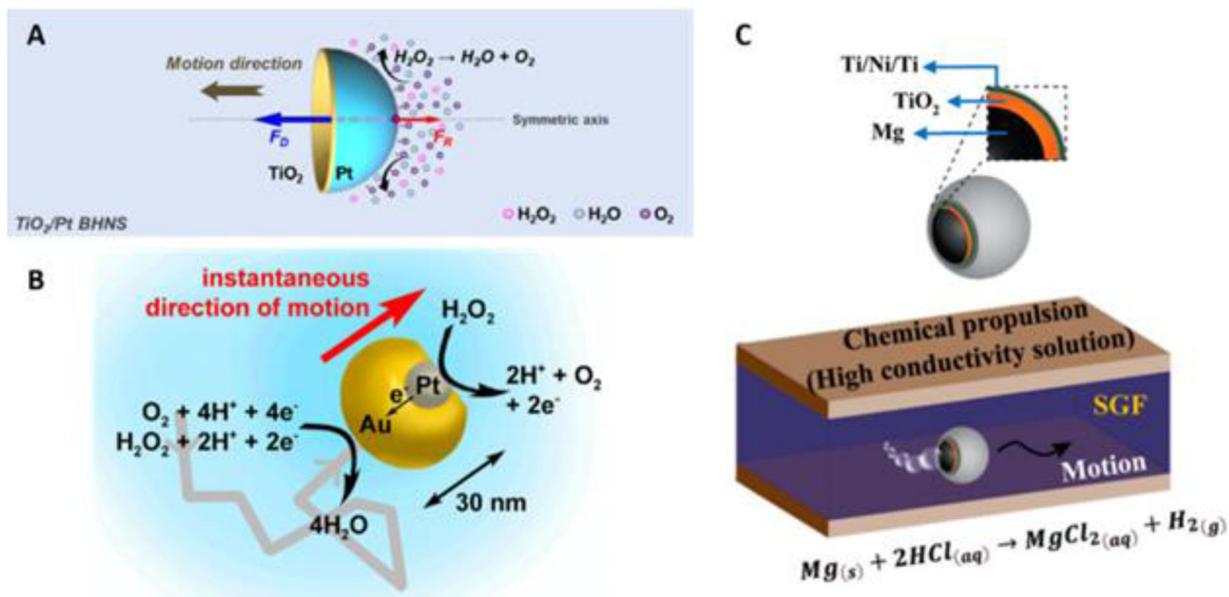
Figure 2. Chemical Propulsion in Solution.
(A) Pt-TiO$_2$ nanoshell undergoing self-diffusiophoresis in solution (reprinted from ref. 15 with permission, copyright 2022, American Chemical Society). **(B)** Au-Pt Janus nanoparticle propelled via self-electrophoresis mechanism (reprinted from ref. 20 with permission, copyright 2014, American Chemical Society). **(C)** Structure (above) of Mg-core micromotor and its movement in solution via bubble propulsion (below) (reprinted from ref. 21 with permission, copyright 2022, American Chemical Society).
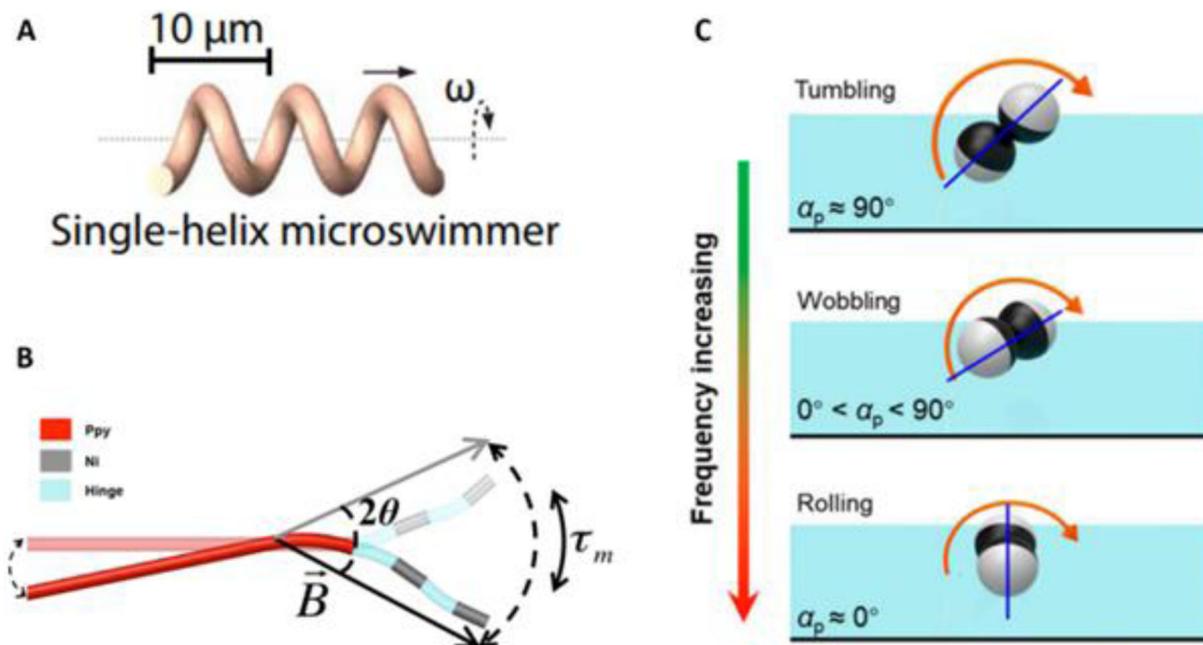
Figure 3. Propulsion via Magnetic Fields Achieved Using Various Geometries.
(**A**) Micro-/nanorobotics can mimic flagellar movements of prokaryotes via use of a helical structure. Application of external magnetic fields help to create corkscrew-like motion (reprinted from ref. 30 with permission, copyright 2021, The American Association for the Advancement of Science). (**B**) Three-link polypyrrole nanoswimmer comprising of magnetic nickel segments connected by flexible polymer heniges (reprinted from ref. 34 with permission, copyright 2015, American Chemical Society). (**C**) Janus microdimer moving via surface-assisted propulsion under a rotating magnetic field (reprinted from ref. 32 with permission, copyright 2021, Frontiers Media S.A.).
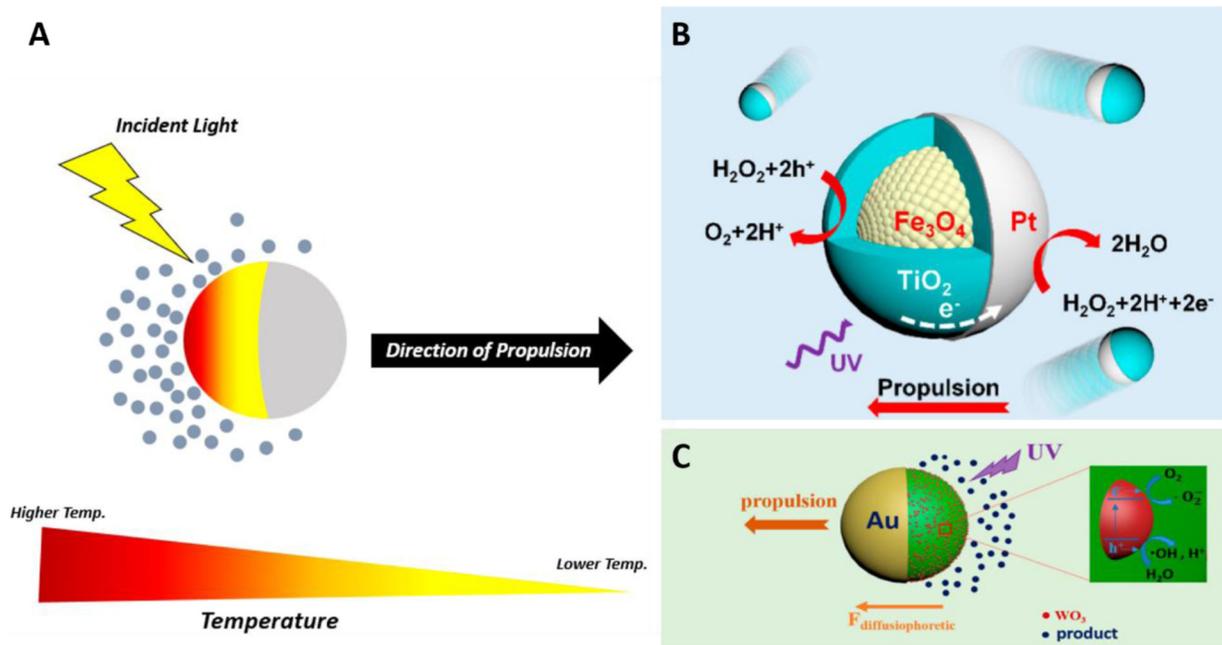
Figure 4. The Main Mechanisms of Light-induced Propulsion of Micro-/Nanorobotics.
(A) Self-thermophoresis. **(B)** Self-electrophoresis (reprinted from ref. 43 with permission, copyright 2022, American Chemical Society). **(C)** Self-diffusiophoresis (reprinted from ref. 44 with permission, copyright 2017, American Chemical Society).
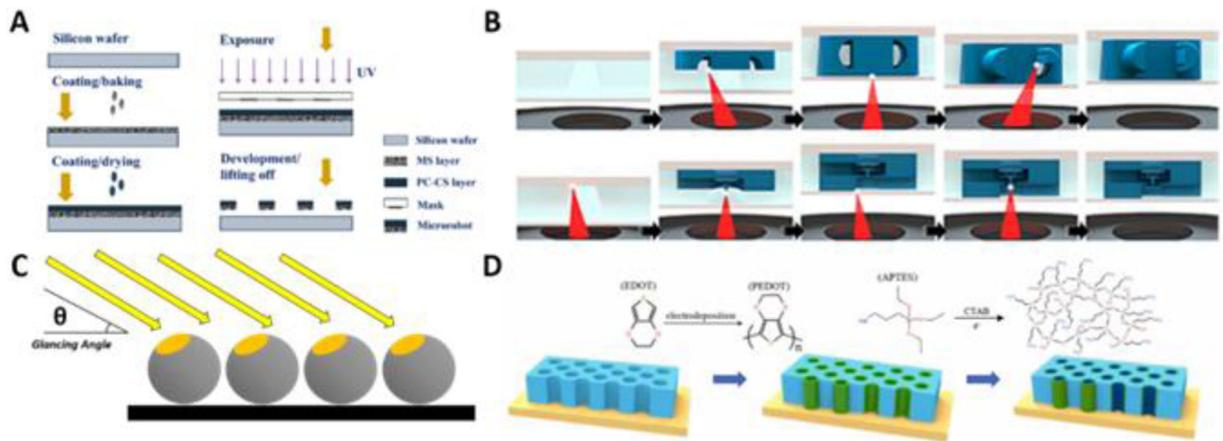
Figure 5. Commonly used Micro-/Nanorobotic Fabrication Methods.
(A) Photolithography (reprinted from ref. 54 with permission, copyright 2022, MDPI).
(B) Additive manufacturing (reprinted from ref. 65 with permission, copyright 2021,
IOP Publishing). **(C)** Glancing angle deposition. **(D)** Template-guided electrodeposition
(reprinted from ref. 59 with permission, copyright 2022, Elsevier B.V.).
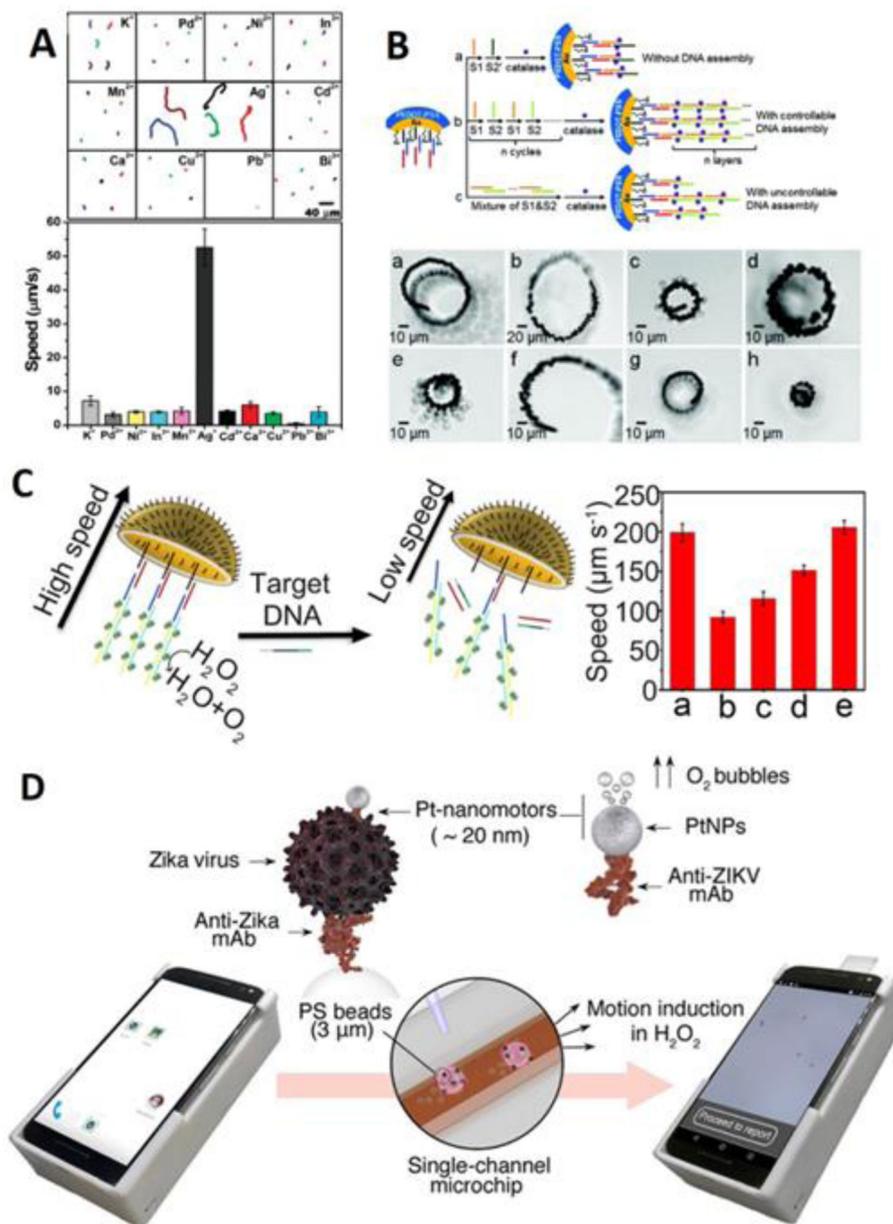
Figure 6. Motion-based sensing.

(A) Motion-based sensing of trace level silver. The reduced silver could accelerate the motion of the nanowire, scale bar: 40 μm (reprinted from ref. 94 with permission, copyright 2009, American Chemical Society). **(B)** Motion-based sensing of DNA improved by cyclic alternate hybridization. The subset of photo from (a) to (h) shows the time-lapse images of micromotors in response to 0, 10, 30, 50, 100, 300, 500 and 1000 nM DNA in 0.2 s, scale bar: 10 μm (reprinted from ref. 102 with permission, copyright 2017, American Chemical Society). **(C)** Motion-based sensing by jellyfish-like micromotor. The plot shows the average speed of micromotor in (a) background, (b) 5 μM target DNA, (c) 50 μM 1 bp mismatch DNA, (d) 50 μM 3 bp mismatch DNA, (d) noncomplementary DNA (reprinted from ref. 103 with permission, copyright 2019, American Chemical Society). **(D)** Motion-based sensing

of Zika virus using smartphone as readout. The screenshots show the motion tracking application interface and data processing (reprinted from ref. 117 with permission, copyright 2018, American Chemical Society).
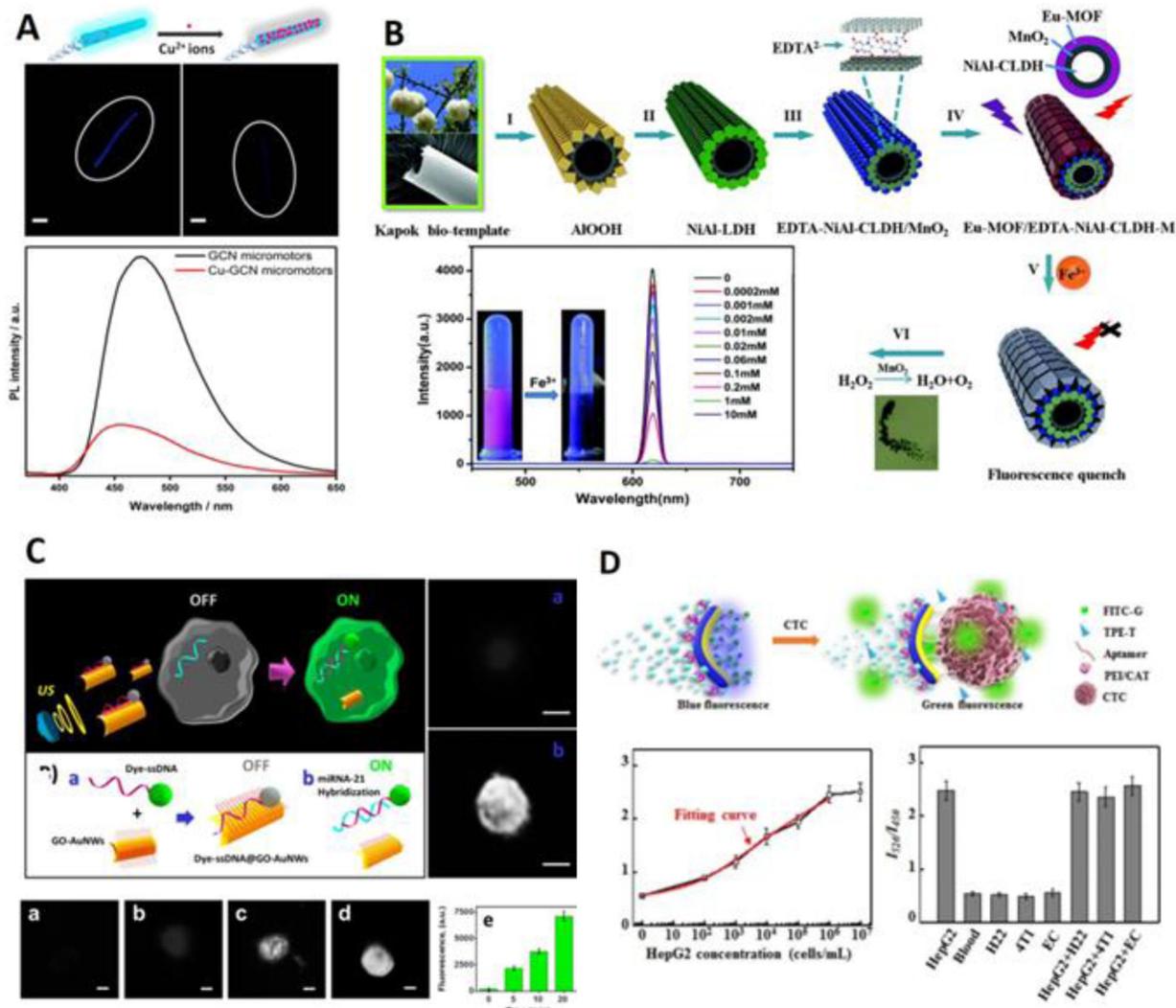
Figure 7. Fluorescence Sensing Based on Micro-/Nanorobotics.
(A) "On-off" fluorescence sensing by copper ion quenching of fluorescence on micromotor, time-lapse images of fluorescence intensity (7 min) (scale bar: 10 μm), and photoluminescence overlapped spectra of micromotor at excitation of 350 nm (reprinted from ref. 122 with permission, copyright 2018, American Chemical Society). (B) Bio-template fabrication of micromotor and the sensing and removal of Fe^{3+}. The inset shows the fluorescence intensity in response to different concentrations of Fe^{3+}(reprinted from ref. 123 with permission, copyright 2019, The Royal Society of Chemistry). (C) "Off-on" fluorescence sensing of miRNA by nanomotor in cell. (a) to (d) fluorescence images of MCF-7 cells after incubation with nanomotor for 0, 5, 10 and 20 min, scale bar: 10 μm. (e) dependence of fluorescence signal upon ultrasound exposure time (reprinted from ref. 128 with permission, copyright 2015, American Chemical Society). (D) Ratiometric fluorescence detection of CTC by Janus micromotor. The insets show the ratio of I_{526}/I_{450} with different concentrations of HepG2 cells (n=3) and the ratio in response to different cells (reprinted from ref. 134 with permission, copyright 2020, Elsevier B.V.).
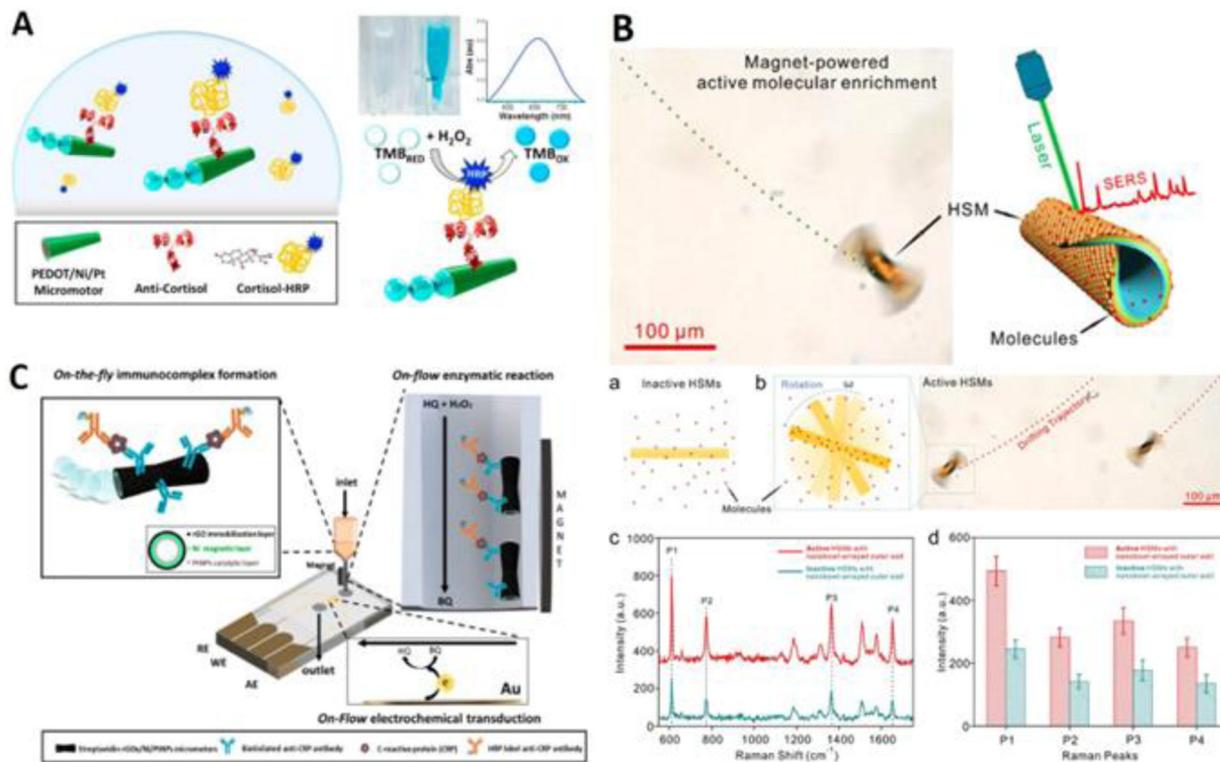
Figure 8. Colorimetric Sensing Based on Micro-/Nanorobotics.
(A) Naked-eye immunoassay of dynamic cortisol by micromotor functionalized with anti-cortisol antibody (reprinted from ref. 142 with permission, copyright 2017, Elsevier B.V.).
(B) Ultrasensitive SERS detection by hotspots engineering on micromotor, scale bar: 100 μm. (a), (b) illustrate the active molecular enrichment by magnet-powered rotation. (c) SERS spectra acquired from passive and active molecular enrichment. (d) SERS intensity of R6G characteristic Raman peak from (c) (reprinted from ref. 152 with permission, copyright 2020, American Chemical Society). **(C)** Illustration showing the electrochemical microfluidic chip for micromotor-based immunoassay of CRP. CRP was first immune-captured by antibody-functionalized micromotor, and then the micromotors were transferred to an electrode for electrochemical transduction (reprinted from ref. 145 with permission, copyright 2020, American Chemical Society).
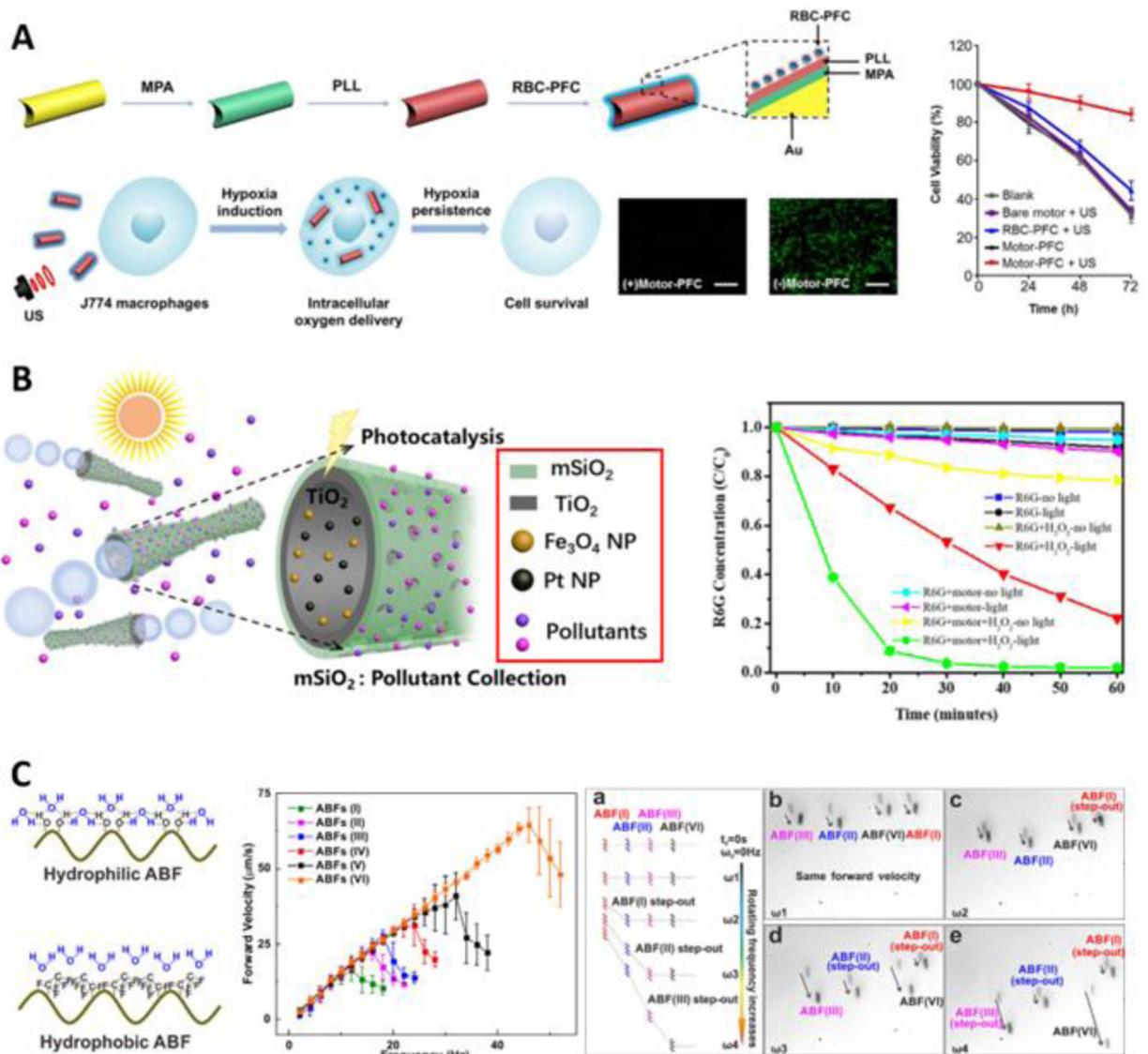
Figure 9. Sensing-based Applications.

(A) Active intracellular oxygen transport by nanomotor. The green fluorescence in the microscope images indicated the intracellular hypoxia stress, indicating that cells treated by the nanomotor maintain low hypoxia stress. Scale bar: 100 μm. The plot shows viability of J774 cells incubated with different concentrations of nanomotor and then subjected to hypoxia (reprinted from ref. 174 with permission, copyright 2019, American Chemical Society). **(B)** Bilayer tubular micromotor for contaminant monitoring and remediation. The outer layer of mesoporous SiO_2 was used for adsorption, and the inner layer of photocatalytic TiO_2 was used for contaminant degradation. The plot shows the degradation of R6G under different conditions (reprinted from ref. 187 with permission, copyright 2018, American Chemical Society). **(C)** Selective manipulation of helical micromotors with different surface hydrophobicity in a swarm. The plot shows the relationship between forward velocity and the rotating frequency of the applied magnetic field for different micromotors. (a) illustrates the selective control of different micromotors, (b) to (e)

screenshots of movement of 4 different micromotors in specific magnetic fields (reprinted from ref. 202 with permission, copyright 2018, American Chemical Society).
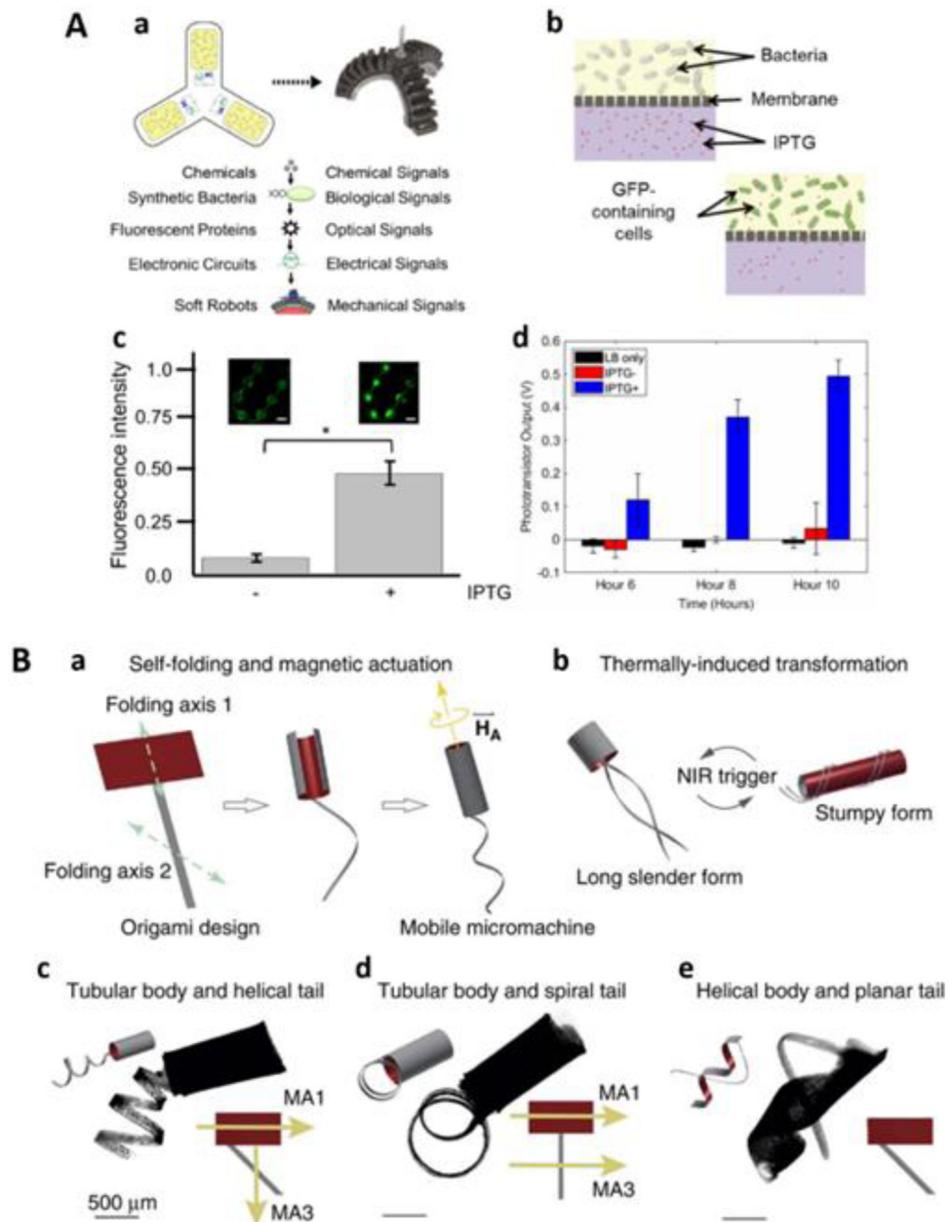
Figure 10. Soft Robotics for Sensing.

(A) A biosensing soft robot. (a) the sensing and actuation mechanism: the synthetic bacteria generated fluorescent protein upon external chemical signals, and the integrated electronic circuits will trigger pneumatic actuation upon the fluorescent signal. (b) the membrane contained pores that allowed the diffusion of chemical signals while retaining bacteria. (c) fluorescence signal from the sealed PDMS layer generated by chemosensitive bacteria in response to IPTG, scale bar: 3 mm. (d) photoresistor output over time in response to IPTG (reprinted from ref. 234 with permission, copyright 2019, The American Association for the Advancement of Science). **(B)** Programmable morphology of soft micromachine. (a) anisotropic swelling controlled by alignment of magnetic nanoparticle and selective patterning of supporting layers led to 3D structure. (b) upon NIR heating, the micromachine

can transform the shape and apply different propulsion mechanism. (c) to (e) show the optical images of soft micromachines with different body shapes. MA1 and MA3 represents magnetic axis in head and tail. Scale bar: 500 μm (reprinted from ref. 244 with permission, copyright 2016, Springer Nature).